

Vision-Language Models for Medical Report Generation and Visual Question Answering: A Review

Iryna Hartsock¹ and Ghulam Rasool¹

¹Department of Machine Learning, H. Lee Moffitt Cancer Center & Research Institute

Abstract

Medical vision-language models (VLMs) combine computer vision and natural language processing to analyze visual and textual medical data. Our paper reviews recent advancements in developing VLMs specialized for healthcare, focusing on models designed for medical report generation and visual question answering. We provide background on natural language processing and computer vision, explaining how techniques from both fields are integrated into VLMs to enable learning from multimodal data. Key areas we address include the exploration of medical vision-language datasets, in-depth analyses of architectures and pre-training strategies employed in recent noteworthy medical VLMs, and comprehensive discussion on evaluation metrics for assessing VLMs' performance in medical report generation and visual question answering. We also highlight current challenges and propose future directions, including enhancing clinical validity and addressing patient privacy concerns. Overall, our review summarizes recent progress in developing VLMs to harness multimodal medical data for improved healthcare applications.

1 Introduction

The last decade has witnessed enormous progress in artificial intelligence (AI) and machine learning (ML), including the development of foundation models (FMs), large language models (LLMs), and vision-language models (VLMs). These AI/ML developments have started transforming several aspects of our daily lives, including healthcare. AI/ML can potentially transform the whole continuum of healthcare by significantly optimizing and improving disease screening and diagnostic procedures, treatment planning, and post-treatment surveillance and care [Baj+21]. Various computer vision (CV) and natural language processing (NLP) models, more recently LLMs, have been instrumental in driving this transformative trend [He+23; Zho+23a]. CV models have been trained and validated for various screening and diagnosis use cases leveraging radiology data from X-rays, mammograms, magnetic resonance imaging (MRI), computed tomography (CT), and others. Recently, AI/ML models focused on digital pathology using histopathology and immunohistochemistry data have also shown significant advances in accurate disease diagnosis, prognosis, and biomarker identification. On the other hand, by training models using large datasets of medical literature, clinical notes, and other healthcare-related text, LLMs are able to extract insights from electronic health records (EHR) efficiently, assist healthcare professionals in generating concise summary reports and facilitate the interpretation of patient information. Noteworthy examples of such LLMs include **GatorTron** [Yan+22], **ChatDoctor** [Li+23c], **Med-PaLM** (Medical Pathways Language Model) [Sin+23] and **Med-Alpaca** [Han+23].

The healthcare data is inherently multimodal, and consequently, the AI/ML models often need to be trained using multiple data modalities, including text (e.g., clinical notes, radiology reports, pathology reports, etc.) imaging (e.g., radiology scans or histopathology slides), and tabular data

(e.g., numerical data such as vitals or labs and categorical data such as race, gender, and others) [Aco+22; Shr+23; Waq+23; Tri+23]. In routine clinical practice, healthcare professionals utilize a combination of these data modalities for diagnosing and treating various conditions. Integrating information from diverse data modalities enhances the precision and thoroughness of disease assessments, diagnoses, treatment planning, and post-treatment surveillance. The need for AI/ML models to ingest, integrate, and learn from information stemming varied data sources is the driving force for *multimodal learning* [Hua+21].

The recent progress in multimodal learning has been driven by the development of *vision-language models (VLMs)* [Gan+22; Che+23]. These cutting-edge models can analyze, interpret, and derive insights from both visual and textual data. In the medical domain, these models are contributing to developing a more holistic understanding of patient information and improving performance of ML models in various clinical tasks. Many of these models, like **CLIP** (Contrastive Language–Image Pre-training) [Rad+21], **LLaVa** (Large Language and Vision Assistant) [Liu+23b], and **Flamingo** [Ala+22] are tailored to healthcare domain through training on extensive medical datasets. Adapting VLMs for medical visual question-answering [Lin+23b] is particularly noteworthy, empowering healthcare professionals to pose queries regarding medical images such as CT scans, MRIs, X-rays, and more. The question-answering capability elevates the interactive nature of the AI/ML models in healthcare, facilitating dynamic and informative exchanges between healthcare providers and the AI system. Furthermore, adapting VLMs for medical report generation enables them to produce detailed and contextually relevant reports by amalgamating information from both visual and textual sources. This not only streamlines the documentation process but also ensures that the generated reports are comprehensive and accurately reflect the subtleties present in the data, further enhancing healthcare workflow efficiency.

1.1 Contribution & Organization

The contribution and organization of this review is as follows:

1. It offers a background on Neural Networks (NNs), Natural Language Processing (NLP), and Computer Vision (CV), ensuring accessibility for readers without a machine learning background (Section 2).
2. It delves into a comprehensive exploration of Vision-Language Models (VLMs), offering detailed insights into their adaptation for downstream tasks (Section 3).
3. It compiles the first and comprehensive list of diverse vision-language datasets used for medical report generation and visual question answering accompanied by detailed dataset descriptions (Section 4).
4. It compiles the first and detailed list of metrics that are used for VLM evaluation (Section 5).
5. It presents a comprehensive review of VLMs specifically tailored for medical report generation and visual question answering, which is the first of its kind to the best of our knowledge. It also includes a comparison of medical VLMs among each other (Section 6).
6. It discusses current challenges in the field and proposes various potential research directions that could significantly shape the future of medical VLMs (Section 7).

The overall structure of this review is shown in Fig. 1.

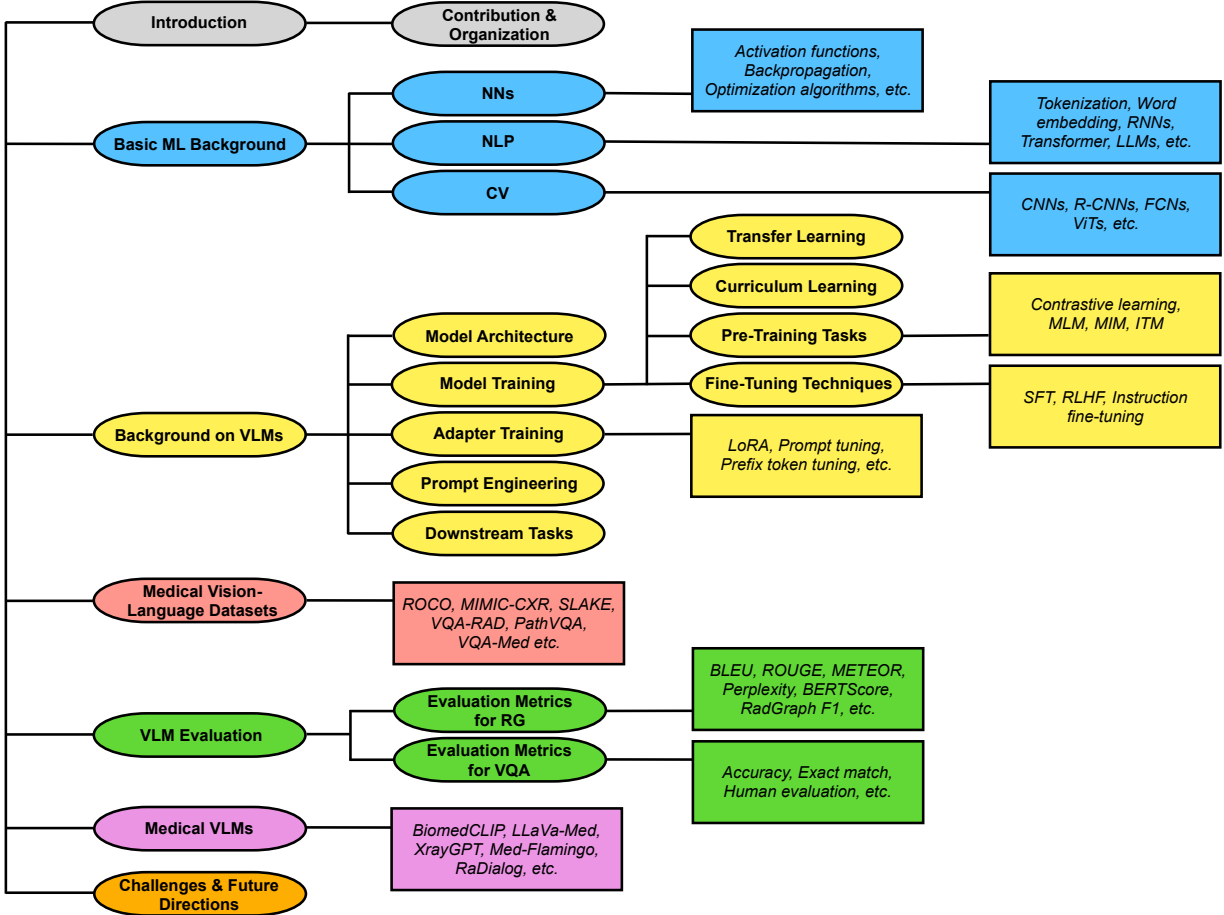


Figure 1: The organization of the review paper.

2 Basic Machine Learning Background

We start this section with a background on neural networks (NNs), natural language processing (NLP) and computer vision (CV).

2.1 Neural Networks

Machine learning (ML) and artificial intelligence (AI), as we understand them today, began to take shape in the late 1940s and early 1950s [Bal21]. *Neural networks (NNs)* stand out as classical machine learning models, drawing inspiration from the structure and functioning of the human brain. They are composed of layers of interconnected *nodes* or *neurons*, arranged into an input layer, an output layer, and multiple intermediate layers called *hidden layers*. The basic NN is a *feedforward NN*, where neurons can be numbered in such a way that a connection from neuron i to neuron j can exist if and only if $i < j$ [Bal21]. In any NN, the connections between nodes carry *weights*, and neurons utilize *activation functions* on their inputs. Activation functions play a crucial role in introducing non-linearity to the model, enabling it to learn complex mappings between inputs and outputs. Common activation functions include the *sigmoid*, *hyperbolic tangent (tanh)*, and *Rectified Linear Unit (ReLU)*. NNs utilize a loss function to quantify the difference between the predicted output and the actual target values. The goal during training is to minimize

this loss.

Backpropagation, short for "backward propagation of errors," is a key algorithm for training deep neural networks. It involves two main steps: forward pass and backward pass. In the *forward pass*, input data is fed through the network, and predictions are generated. The *backward pass* calculates the gradient of the loss function with respect to the weights of the network. This gradient is then used to update the weights, minimizing the difference between predicted and actual values. Backpropagation is a straightforward application of the chain rule for computing derivatives [Bal21]. After the backward pass, the *optimization algorithm* takes these gradients and adjusts the weights and biases of the NN to minimize the loss. Among common optimization methods are *stochastic gradient descent (SGD)* [Rob51] and *Adam (Adaptive Moment Estimation)* [KB14].

In practice, several issues can be encountered when training NNs. The *vanishing gradient problem* arises when gradients become extremely small as they are propagated backward through the layers during training. As a result, the weights in the early layers of the network receive negligible updates, hindering their learning. This phenomenon is particularly problematic for deep architectures with many layers. To tackle this issue, ReLU activation functions or skip connections, as proposed in **ResNet** [He+16], are commonly utilized. Another common issue is the *exploding gradient problem*. This occurs when gradients become excessively large during backpropagation, leading to unstable training and convergence issues. To address exploding gradients, techniques such as gradient clipping, which involves scaling gradients if they exceed a certain threshold, are employed. Moreover, overfitting and underfitting are common issues in NN training. *Overfitting* occurs when the model performs well on the training data but poorly on new, unseen data, indicating that it has memorized the training set rather than learning the underlying patterns. Increasing model complexity is a common strategy to address overfitting. On the other hand, *underfitting* arises when the model's performance is poor on both the training and testing data, indicating a failure to capture the underlying patterns in the data. To mitigate these problems, regularization methods such as dropout, which randomly drops neurons during training to prevent reliance on specific features, are commonly employed [Bal21].

2.2 Natural Language Processing

Natural Language Processing (NLP) is the analysis of linguistic data, most commonly in the form of textual data such as documents or publications, using computational methods [VC13]. NLP encompasses a variety of tasks aimed at understanding, processing, and generating human language. *Named entity recognition (NER)*, a prominent NLP task, focuses on identifying and classifying entities within the text, such as names of individuals, medical conditions, etc. For instance, in medical literature, NER can assist in extracting crucial information from documents. *Text summarization* in NLP is widely used for generating coherent summaries of lengthy texts. *Sentiment analysis* is a task that determines the emotional tone expressed in a given text, providing valuable insights for applications like social media monitoring or customer feedback analysis. *Machine translation* is a fundamental NLP task in breaking down language barriers by automatically translating text from one language to another. *Question answering* in NLP is directed at comprehending and responding to user queries, propelling advancements in virtual assistants and information retrieval.

The first step in NLP is tokenization, which is the mechanism of splitting or fragmenting the sentences and words to their possible smallest morpheme called a token. A morpheme is the smallest possible word after which it cannot be broken further [RB21]. One example of a word-level tokenization method is *whitespace tokenization*, which segments text based on whitespace characters. In many NLP applications, subword tokenization methods are preferred due to their effectiveness in handling out-of-vocabulary words. *WordPiece* [Wu+16] begins by treating each

character as a token, creating an initial vocabulary. Employing a flexible and adaptive merging strategy, WordPiece considers any pair of adjacent characters or subword units that enhance the overall likelihood of the training data. This likelihood reflects the model’s probability of accurately representing the training data given its current state. In contrast, *Byte Pair Encoding (BPE)* [SHB16] shares similarities with WordPiece but adheres to a more deterministic merging strategy. In each iteration, BPE merges the most frequent pair of adjacent characters or subword units, progressing toward a predefined vocabulary size. *Byte level BPE* [WCG20] operates at an even finer granularity, considering individual bytes rather than characters. Byte Level BPE extends the concept of subword tokenization to bytes, allowing it to capture more nuanced patterns at the byte level.

Tokens are then often transformed into numerical vectors that capture semantic relationships; this feature extraction is called a *word embedding*. Word embeddings are commonly used in tasks where understanding the meaning of words in context is crucial, for example, in sentiment analysis, named entity recognition, and language translation. *Word2Vec* [Mik+13a] is a widely used word embedding technique that uses two models: *Skip-Gram* [Mik+13b] and *Continuous Bag of Words (CBOW)* [Mik+13c]. In Skip-Gram, the model predicts context words given a target word, capturing semantic associations. Conversely, CBOW predicts the target word based on its context, emphasizing syntactic structures. In both models, the “context word” refers to words within a specified window around the target word, and the “target word” is the word for which predictions are made. Word2Vec is computationally efficient, making it well-suited for large datasets and general-purpose applications. *GloVe (Global Vectors)* [PSM14] is a word embedding model that distinguishes itself by capturing global semantic relationships. It focuses on the entire corpus rather than local context windows. The model builds a co-occurrence matrix based on the global statistics of word pairs and then employs an objective function to generate word vectors that reflect the ratio of co-occurrence probabilities. GloVe uses an implicit Skip-Gram approach, capturing word relationships globally, making it ideal for tasks that demand a holistic understanding of word connections. *FastText* [Boj+17] is another word embedding that is particularly effective for handling out-of-vocabulary words and morphologically rich languages. It adopts a sub-word approach, breaking words into “n-grams”, and employs a Skip-Gram training method similar to Word2Vec [Mik+13a] to learn embeddings for these sub-word units. There are also word embeddings tailored to better represent biomedical and clinical terms. In tasks where the order of words is not essential other feature extraction techniques can be effective, for example, *bag-of-words (BoW)* in text classification or *term frequency-inverse document frequency (tf-idf)* for information retrieval.

In addition to general-purpose word embeddings, there are ones designed for biomedical and clinical terms. *BioWordVec* [Zha+19] incorporates MeSH (Medical Subject Headings) terms along with text from PubMed abstracts and employs the fastText [Boj+17] algorithm to learn improved biomedical word embeddings. Another prominent approach is *Cui2vec* [Bea+20], which leverages diverse multi-modal data derived from medical publications and clinical notes. Cui2vec systematically maps medical terms onto a common Concept Unique Identifier (CUI) space, followed by the construction of a co-occurrence matrix. This matrix captures instances where different CUIs appear together, which is a foundation for generating word embeddings using techniques such as GloVe [PSM14] or Word2Vec [Mik+13a]. It’s worth noting that, post word embedding extraction, the incorporation of *positional encodings* becomes common to address the challenge of representing the order of elements in a sequence. These encodings, often based on sinusoidal functions, systematically encode token positions, enriching embeddings with positional information for utilization in machine learning models tailored to specific NLP tasks.

Recurrent Neural Networks (RNNs) are widely employed for pattern detection in sequential data, encompassing diverse types such as genomic sequences, text, or numerical time series [Sch19].

Operating on the principle of preserving a form of memory, RNNs incorporate a cyclic structure by looping the output of a specific layer back to the input, facilitating the prediction of subsequent layer outputs. This mechanism empowers RNNs to adeptly model sequential and temporal dependencies, capturing information from preceding time steps within hidden states. Despite their capacity to retain information from past inputs, RNNs encounter challenges in preserving long-term dependencies within input sequences due to the vanishing gradient problem. To address this, several RNN variants, including *Long Short-Term Memory (LSTM)* [HS97] and *Gated Recurrent Unit (GRU)* [Cho+14] networks, have been designed to enhance their ability to capture and utilize long-range dependencies in sequential data.

In recent years, there has been a remarkable advancement in NLP mainly due to the development of the *Transformer* [Vas+17]. Beyond incorporating embedding layers and positional encodings, the Transformer architecture consists of an *encoder* that processes input data, represented by vectors obtained from embedded and positionally encoded tokens. The encoder-generated representation then serves as the input for the subsequent *decoder*, which transforms these vector representations into a relevant output tailored to the specific task at hand. A defining characteristic of the Transformer lies in its *self-attention mechanism*, notably the scaled dot-product attention, which proves instrumental in capturing intricate dependencies within sequences. This mechanism, employed in both the encoder and decoder, utilizes queries and keys during the attention process. *Queries* serve as projections of the input sequence, encapsulating information for attending to other positions, while *keys* represent the positions within the sequence. Enhanced by *multi-head attention* for parallelization, the self-attention mechanism enables the model to dynamically weigh different parts of the input sequence, fostering a nuanced understanding of contextual relationships. The incorporation of potent GPUs significantly amplifies these capabilities, ensuring swift and efficient computations. Furthermore, each layer in both the encoder and decoder encompasses sub-layers, including a *feedforward NN*, further augmenting the model's capacity to capture intricate patterns within the data. In practice, Transformers face limitations in effectively processing long sequences and exhibit less selectivity about relevant information when considering all positions in the sequence. To address these issues, various techniques have been proposed. One such approach, known as *hierarchical attention* [Yan+16], strategically reduces computational complexity and enhances contextual sensitivity, by initially computing attention at the word level, and then at the sentence level. Another notable advancement in attention algorithms is the *FlashAttention-2* [Dao23], designed to significantly accelerate attention computations.

The synergy between the enhanced computational power provided by GPUs and the advancements in attention mechanisms has played a pivotal role in the development of *large language models (LLMs)*. These models are meticulously trained on vast datasets, accumulating a substantial number of parameters, including weights and biases within the neural network. Initial LLMs include, but are not limited to, **BERT** (Bidirectional Encoder Representations from Transformers) [Dev+19] (the largest version comprising 235 M parameters), **ALBERT** (A Lite BERT) [Lan+19] (with the largest variant at 12 M parameters), and **Megatron-LM** [Sho+19] (the largest version featuring 1.2 B parameters). The era of even larger LLMs began in 2020, introducing models like **GPT-3** (the 3-generation Generative Pre-trained Transformer) [Bro+20] (175 B parameters) and **PaLM** (Pathways Language Model) [Cho+22] (540 B parameters). Some of the most recent LLMs are **LLaMA** (Large Language Model Meta AI) [Tou+23b], **Vicuna** [Chi+23], **Llama 2** [Tou+23a], and **Mistral** [Jia+23]. Note that LLMs can also be used to generate word embeddings (e.g., **BERT** [Dev+19]).

2.3 Computer Vision

Computer vision (CV) involves interpreting and understanding the world from their images or videos [Ji20]. Data in CV is encoded as numerical values representing the intensity or brightness of pixels. The extraction of visual patterns like edges, textures, and objects in images or video frames serves as building blocks for various CV tasks. *Image classification* is the task of assigning a label to an entire image, determining the main object or scene. *Object detection* involves identifying and locating multiple objects within an image, providing both labels and bounding boxes. *Image segmentation* divides an image into meaningful segments, assigning a label to each pixel and outlining the boundaries of distinct objects or regions. Various machine learning techniques and models are utilized for these tasks [Mah+22].

The *Convolutional Neural Networks (CNNs)* [Yam+18] represents a significant advancement in CV, especially in image classification. Besides pooling and fully connected layers, CNNs have also convolution layers, which are instrumental in applying convolution operations. During a convolution operation, a small filter or kernel slides over the input data. At each position, the filter performs element-wise multiplications with the local regions of the input. The results of these multiplications are then summed, creating a new value in the output feature map. This process is repeated across the entire input, capturing patterns and features at different spatial locations. A commonly used CNN architecture is **ResNet** (Residual Network), or **RN** [He+16], which diverges from traditional NNs by focusing on learning the differences (residuals) between desired and actual outputs at each layer. This innovative approach aids in training exceptionally deep NNs by mitigating the vanishing gradient problem, providing shortcuts for more effective gradient flow throughout the network. Another popular CNN is **DenseNet** (Dense Convolutional Network) [Hua+19]. In its architecture, each layer receives feature maps from all preceding layers as input, and it, in turn, provides its feature maps as input to all subsequent layers. This dense connectivity pattern promotes feature reuse, and parameter efficiency, and enhances the network's ability to capture intricate patterns across different scales. **EfficientNet** [TL20] represents a CNN architecture with a unique scaling method that uniformly scales network width, depth, and resolution in a balanced manner. This approach allows the network to achieve improved performance while maintaining computational efficiency.

A pivotal advancement in object detection has been the emergence of *R-CNNs (region-based CNNs)* [Gir+14]. The primary objective of R-CNNs (e.g., **faster R-CNN** [Ren+15]) is to not only categorize objects but also precisely determine their spatial location in an image with a bounding box. Contrary to traditional CNNs, which analyze the entire image in a single pass, R-CNNs utilize a three-step approach. First, potential regions of interest, called *region proposals*, are extracted (e.g., using a *selective search* or a *region proposal network*). Next, each region is fed into a CNN, and then the output feature vectors are classified (e.g., by the *support vector regression (SVM)*). R-CNN models show a high accuracy performance, especially for larger objects. Another known object detection model is **YOLO** (You Only Look Once) [Red+16], which divides an image into a grid and predicts bounding boxes and class probabilities for each grid cell in a single forward pass. This approach enables the model to detect multiple objects in an image simultaneously with higher speed which makes it a popular choice for real-time applications.

The CNNs have also revolutionized image segmentation. **Mask R-CNN** [He+17], an extension of **faster R-CNN** [Ren+15], introduces an additional branch dedicated to outlining precise pixel-level segmentation for each object instance. **U-Net** [RFB15], featuring a U-shaped structure, proves especially popular in biomedical fields. The architecture is characterized by a contracting path responsible for capturing context and extracting features from the input image (encoding) and an expansive path that facilitates precise localization and segmentation of objects (decoding).

Moreover, *Fully Convolutional Networks (FCNs)* (e.g., **FastFCN** [Wu+19]), represent a category of CNNs where traditional fully connected layers are replaced with convolutional layers, making them exceptionally well-suited for image segmentation tasks.

Transformer models which were originally designed for NLP tasks, have also found valuable applications in CV. For instance, *vision transformers (ViTs)* [Dos+21] can capture intricate relationships and dependencies across the entire image. This is achieved by leveraging the Transformer architecture and treating images as sequences of smaller patches. Here, each image patch undergoes a process of flattening into a vector, followed by passage through an embedding layer. The embedding layer enriches the flattened image patches, providing a more expressive and continuous representation. Next, positional encodings are incorporated into the embeddings, conveying information about the spatial arrangement of the image patches. A distinctive feature of ViTs is the introduction of a *special token* designed to capture global information about the entire image. This special token has an associated learnable token embedding, represented by a vector with its unique set of parameters. ViTs have achieved notable success in segmentation [RBK21], anomaly detection [Mis+21], medical image classification [Man+23] and even outperformed CNNs in some cases [Tya+21; Xin+22].

3 Background on Vision-Language Models

Many real-world situations inherently involve a variety of data *modalities*. For example, autonomous cars must process information from various sensors like cameras, RADAR, and GPS to ensure safe and effective navigation [Par+22]. Similarly, in oncology, the amalgamation of radiology images with genomic data, histopathology images, and clinical reports has the potential to greatly refine the precision of cancer diagnoses [Boe+21]. This motivated the development of VLMs, which can handle and understand both NLP and CV data simultaneously.

3.1 Model Architecture

Based on how different modalities are fused in VLMs, they are generally categorized into two groups [Che+23]: (1) *single-stream* (e.g., **VisualBERT** [Li+19], **UNITER** (UNiversal Image-Text Representation Learning) [Che+19]), and (2) *dual-stream* models (e.g., **ViLBERT** (Vision-and-Language BERT) [Lu+19], **CLIP** [Rad+21]).

A single-stream VLM adopts an efficient architecture for processing both visual and textual information within a unified module. This architecture incorporates an early fusion of distinct modalities, where feature vectors from various sources are concatenated into a single vector (e.g., **MedViLL** [Moo+22]). Subsequently, this combined representation is fed into a single stream. One notable advantage of the single-stream design is its parameter efficiency, achieved by employing the same set of parameters for all modalities. This not only simplifies the model but also contributes to computational efficiency during both training and inference phases [Che+23].

In contrast, a dual-stream VLM extracts visual and textual representations separately in parallel streams that do not share parameters. This architecture usually has higher computationally complex compared to single-stream architectures. Visual feature vectors are generated from pre-trained *vision encoders*, such as CNNs, R-CNNs, or ViTs, and textual feature vectors are obtained from pre-trained *text encoders*, usually based on a Transformer architecture (e.g., **PubMedCLIP** [EMD23]). They are then inputted into a *multimodal fusion module*, often leveraging attention mechanisms, to integrate information from both modalities and to create cross-modal representations. This late fusion approach allows for more intricate interactions between visual and textual

information, enabling the model to capture complex cross-modal dependencies. However, it comes at the cost of increased computational complexity compared to single-stream architecture.

In addition, modality-combined representations may be optionally forwarded into a *decoder* before producing the final output. Consequently, VLMs are classified into two groups: (1) *encoder-only* (e.g., **ALIGN** (A Large-scale ImaGe and Noisy-text embedding) [Jia+21]), and (2) *encoder-decoder* models (e.g., **SimVLM** (Simple Visual Language Model) [Wan+22c]). Encoder-only models are advantageous in scenarios where the primary objective is efficient representation learning. They often exhibit streamlined processing and reduced computational complexity, making them suitable for tasks requiring compact and informative representations. However, these models might lack the capability to generate intricate and detailed outputs, limiting their use in tasks demanding nuanced responses or creative generation. On the other hand, encoder-decoder models offer the flexibility to generate complex and diverse outputs, making them well-suited for tasks like image captioning, translation, or any application requiring creative responses. The decoding step allows for the transformation of joint representations into meaningful outputs. However, this versatility comes at the cost of increased computational load and complexity.

3.2 Model Training

In this section, we discuss strategies for adapting VLMs through full or partial model updates.

3.2.1 Transfer Learning

In the realm of VLMs and the broader scope of machine learning, a commonly adopted strategy is to employ pre-trained models and customize them to specific downstream tasks, a method commonly known as *transfer learning*. This process typically involves fine-tuning the model’s parameters using smaller task-specific datasets to address the intricacies of the target task. Moreover, during fine-tuning, one may adjust the model’s architecture. This can include modifications to the final layers or the introduction of new layers, such as classification or regression layers, tailored to meet the specific requirements of the task at hand. The underlying idea is to adapt the pre-trained model to the specifics of the new task while retaining the knowledge it gained during the initial pre-training.

3.2.2 Curriculum Learning

Curriculum learning [Sov+21] presents an innovative approach when dealing with tasks or data exhibiting a natural progression or hierarchy. This method involves strategically presenting training examples or tasks in a designed order, typically based on difficulty or complexity measures. The recent VLM, **LLaVa-Med** [Li+23a], adopts curriculum learning during its training phase. This allows the model to learn gradually, starting with simpler examples and progressing to more intricate ones. This orchestrated learning sequence enhances the model’s adaptability and performance.

3.2.3 Pre-Training Tasks

The pre-training process plays a pivotal role in equipping VLMs with a foundational understanding of the intricate interplay between visual and textual data. A prevalent strategy involves intensive pre-training on datasets where images/videos are paired with their corresponding textual descriptions. During pre-training, various tasks guide the model in learning versatile representations for downstream tasks.

One prevalent task is *contrastive learning (CL)*, a technique that encourages the model to learn meaningful representations by contrasting positive pairs with negative pairs of both visual and textual data [Li+21]. In contrastive learning, the model is trained to map both positive and negative pairs into a shared embedding space. Positive pairs consist of examples where the visual and textual content are related, such as an image paired with its corresponding textual description. Conversely, negative pairs consist of examples where the visual and textual content are unrelated, like an image paired with a randomly selected different textual description. The objective is to maximize the distance between positive pairs while maximizing the distance between negative pairs in the shared embedding space. Several contrastive loss functions are used in contrastive learning to achieve this objective. Various contrastive loss functions are employed to achieve this objective, with the *InfoNCE (Noise-Contrastive Estimation) loss* [OLV19] being a common choice. InfoNCE formulates a probabilistic task where the model is trained to maximize the likelihood of observing positive pairs and minimize the likelihood of observing negative pairs. The negative log-likelihood of the positive pair is used as the loss. The **CLIP** [Rad+21] employs InfoNCE loss with cosine similarity. Other VLMs deviate from InfoNCE, for instance, **ALIGN** [Jia+21] uses a *normalized softmax loss*. This loss computes the softmax over cosine similarities between the normalized embeddings of positive and negative pairs, aiming to boost positive similarity while diminishing negative similarities.

In NLP pre-training, a widely used task is *masked language modeling (MLM)* [Tay53]. It was first introduced and applied in the **BERT** model [Dev+19]. MLM involves randomly selecting a percentage of tokens within textual data and replacing them with a special token, often denoted as MASK. The model predicts these masked tokens by taking into account the context on both sides of them, allowing the model to grasp nuanced contextual information. VLMs such as **UNITER** [Che+19] and **VisualBERT** [Li+19] leverage MLM for pre-training. Extending this idea to images gave rise to *masked image modeling (MIM)* [Xie+22]. Within MIM, certain patches are masked, prompting the model to predict the content of masked regions. This process enables the model to draw context from the entirety of the image, encouraging the integration of both local and global visual features. VLMs like **UNITER** [Che+19] and **ViLBERT** [Lu+19] leverage MIM for enhanced performance. The *cross-entropy loss* is employed in MLM and MIM tasks to measure the difference between predicted and actual probability distributions for the masked elements. Additionally, MLM can be combined with MIM, allowing the reconstruction of the masked signal in one modality with support from another modality [Kwo+23].

Self-supervised learning [Ran+23a] is a fundamental paradigm in training VLMs, offering a powerful alternative to traditional supervised learning by allowing models to generate their own labels from the data. This is particularly beneficial when obtaining large amounts of labeled data is challenging or expensive. In self-supervised learning for VLMs, the models formulate tasks that leverage inherent structures within the data, enabling them to learn meaningful representations across modalities without explicit external labels. CL, MLM, and MIM are examples of self-supervised learning tasks.

Another common vision-language pre-training task is *image-text matching (ITM)*. Throughout the training, the model learns to map images and corresponding textual descriptions into a shared semantic space, where similar content in both modalities is represented by closely aligned vectors. In single-stream VLMs, the special token [CLS] represents the joint representation for both modalities, while in dual-stream VLMs, the visual and textual representations of $[\text{CLS}]_V$ and $[\text{CLS}]_T$ are concatenated. This joint representation is input into a fully-connected layer and a sigmoid function, predicting a score indicating match or mismatch [Che+23]. Models like **CLIP** [Rad+21], **ALBEF** (ALign the image and text representations BEfore Fusing) [Li+21], and **METER** [Dou+22] leverage ITM during pre-training.

In VLM pre-training, multiple tasks are often combined in a unified framework, allowing models to grasp nuanced contextual information across modalities. The final loss function can combine contrastive loss, cross-entropy loss for masked token prediction, and other task-specific losses. This comprehensive pre-training approach equips VLMs with versatile representations for diverse downstream tasks. For example, **ALBEF** [Li+21] adopts a comprehensive pre-training objective encompassing three tasks: CL, MLM, and ITM. The overall loss is then computed as the sum of these individual components.

3.2.4 Fine-Tuning Techniques

Following the training of VLMs, a common practice involves *fine-tuning* them on smaller datasets tailored to specific downstream tasks. One fine-tuning approach in the context of ITM pre-training is known as *supervised fine-tuning (SFT)*. In the initial phase, the model undergoes pre-training on an extensive image-text dataset, establishing a foundational understanding of the complex interplay between visual and textual components. Subsequently, meticulous fine-tuning takes place on a more focused dataset, curated to match the nuances of the targeted application. This dual-phase strategy, encompassing broad pre-training and task-specific fine-tuning, enables the model to benefit from large-scale generalization while seamlessly adapting to the intricacies of particular applications.

In contrast, *reinforcement learning from human feedback (RLHF)* is a distinct fine-tuning approach employed to enhance VLMs through a systematic sequence of steps. Initially, an existing VLM serves as the foundation, with the option for potential fine-tuning using additional textual data. Subsequently, a detailed reward model is constructed by ranking text outputs generated by the VLM based on human preferences. The fine-tuning phase employs a policy-gradient reinforcement learning algorithm, such as *Proximal Policy Optimization (PPO)*, to adjust the VLM’s parameters. The reward function combines scalar rewards from the trained model with a penalty mechanism that discourages substantial deviations from the pre-trained model. This iterative process ensures the optimization of the VLM, tailoring it to specific visual and textual tasks, aligning it with human preferences, and thereby enhancing its overall performance and adaptability.

Instruction fine-tuning refers to the process of refining a pre-trained language model by providing specific instructions or guidance tailored to a particular task or application. This process typically involves exposing the model to examples or prompts related to the desired instructions and updating its parameters based on the feedback received during this task-specific training phase. **RaDialog** [Pel+23] employs this fine-tuning technique.

3.3 Adapter Training

In this section, we explore strategies for adapting VLMs while keeping the model’s parameters frozen and only updating newly added layers.

In recent years, *parameter-efficient fine-tuning (PEFT)* has gained prominence, encompassing various techniques and strategies that aim to make the most effective use of parameters during the fine-tuning process, particularly in scenarios with limited labeled data for the target task. One strategy is incorporating task-specific parameters, known as *adapters*, into a pre-trained model while retaining its original parameters. The architecture of adapter modules typically incorporates a bottleneck structure, projecting original features into a reduced dimension, applying non-linearity, and then projecting back to the original dimension. This thoughtful design ensures parameter efficiency by limiting the number of added parameters per task. Integrated after each layer of the pre-trained model, adapter modules capture task-specific details while preserving shared parameters, enabling the model’s seamless extension to new tasks without significant interference with

previously acquired knowledge.

The common adapter-based method is *low-rank adaptation (LoRA)* [Hu+22]. In LoRA, the adaptation process involves fine-tuning two smaller matrices that approximate the larger weight matrix of the pre-trained language model. These smaller matrices constitute the LoRA adapter modules, and the approach focuses on making low-rank modifications to efficiently adapt the model for specific tasks. Pre-trained LLMs that are part of medical VLMs architecture are often fine-tuned using LoRA (e.g., **Visual Med-Alpaca** [Shu+23] and **RaDialog** [Pel+23]).

Prompt tuning [LAC21] involves creating continuous vector representations as input hints. This allows the model to dynamically generate effective prompts during training. Continuous refinement of prompts significantly enhances the model’s ability to generate accurate and contextually relevant responses. This iterative process allows the model to adapt its behavior based on an evolving understanding of the task. Prompt tuning was used by VLMs like **Qwen-VL** [Bai+23] and **InstructBLIP** [Dai+23].

Prefix token tuning [LL21] adds task-specific vectors to the input, specifically to the initial tokens known as *prefix tokens*, to guide the model’s behavior for a given task. For instance, **VL-T5** [Cho+21] utilized different prefixes for questions from various datasets. These vectors can be trained and updated independently while keeping the remaining pre-trained model parameters frozen. Prefix token tuning allows for task-specific adaptation without compromising the pre-trained knowledge encoded in the majority of the model’s parameters.

3.4 Prompt Engineering

In this section, we explore strategies for adapting VLMs while keeping the model’s parameters frozen and refraining from any updates.

Prompt engineering [Gu+23] is a technique that involves enhancing a large pre-trained model with task-specific instructions, referred to as *prompts*, to tailor the model for specific tasks. Examples include instructing the model to generate a radiology report for a specific image (e.g., **RAMM** [Pel+23]). Prompt engineering can also expose the VLM to a sequence of interconnected examples or prompts, guiding it to a desired output. Another approach is to incorporate progressively structured instructions or questions, refining focus and enhancing the model’s ability to generate coherent and contextually relevant responses.

Retrieval augmented generation (RAG) is a form of prompt engineering that involves strategically crafting prompts for both retrieval and generation phases, allowing for an adaptive and efficient process that leverages external knowledge sources to enhance generative tasks. While the original concept of RAG was developed in the context of NLP [Lew+20], the principles behind retrieval and generation can be extended to multimodal learning [Zha+23d], including VLMs. RAG has been used in vision-language tasks like VQA (e.g., **RAMM** [Yua+23]) and RG (e.g., **CXR-RePaiR-Gen** [Ran+23b]). RAG begins with a retrieval component, which is usually a pre-trained model designed for information retrieval. This versatile component excels in extracting pertinent information from extensive datasets, catering to various modalities such as images, text, codes, video, or audio when presented with diverse inputs [Zha+23d]. Following the retrieval phase, the model returns a set of contexts related to the given input. The second component is a generative language model, often based on architectures like **GPT**. This component takes the input and the retrieved context and generates the final output. The generated output is conditioned not only on the input but also on the information extracted from the retrieved context. An intrinsic advantage of RAG lies in its capacity to reduce the reliance on extensive labeled datasets. By tapping into external knowledge sources, the model becomes more data-efficient and adept at handling a spectrum of tasks. While the base model is typically frozen during RAG, there are instances, as seen

in **RAMM** [Yua+23], where model parameters are updated in the process.

3.5 Downstream Tasks

Multimodal downstream tasks leverage the acquired knowledge from pre-training VLMs to excel in diverse applications that require a joint understanding of visual and textual data. A prominent example is *report generation (RG)* task, which centers on creating a comprehensive summary report of visual data. In the medical domain, RG plays a crucial role in automatically summarizing diagnostic imaging results and reducing the workload of report writing [TLZ23]. For instance, in radiology, a report generation system could analyze a set of medical images such as X-rays, CT scans, or MRIs, and generate a detailed report summarizing the observed abnormalities, their locations, and potential implications for diagnosis or treatment [LTS23]. A radiology report usually has several sections: *Examination* (type of exam), *Indication* (reasons for the examination), *Comparison* (prior exams), *Technique* (scanning method) *Findings* (detailed observations made by a radiologist), and *Impression* (summary of the major findings) [MHC20]. In the context of RG, VLMs are usually designed to generate Findings and Impression sections [Tha+23]. Currently, VLMs tailored for RG are predominantly utilized for radiology images, with lesser application in other medical imaging domains such as histopathology [SB23], robotic surgery [Xu+21], and ophthalmology [Li+22].

Another significant visual-language understanding task is *visual question answering (VQA)*, where the model needs to comprehend images or videos and the posed question to provide a relevant and accurate response [Ant+15]. The spectrum of questions encountered in VQA is broad, encompassing inquiries about the presence of specific objects, their locations, or distinctive properties within the image. In a medical context [Lin+23b], this may involve questions regarding the presence of medical conditions or abnormalities, such as “What abnormality is seen in the image?” [Ion+21] or “Is there gastric fullness?” [Lau+18]. Other queries may delve into details like the imaging method used [Aba+19], the organ system involved [Lau+18], or the presence of specific anatomical structures [Liu+21a].

Questions in VQA fall into two categories. *Open-ended questions* elicit responses in the form of phrases or sentences, fostering detailed and nuanced answers [Tha+23]. On the other hand, *closed-ended questions* are designed to prompt limited responses, often with predetermined options, such as a short list of multiple choices, a yes/no response, or a numeric rating [Baz+23]. The task of VQA is commonly approached as either a *classification* task or a *generation* task or both [Lin+23b]. In the classification approach, models select the correct answer from a predefined set, while in the generation task, models produce free-form textual responses unconstrained by predefined options.

Beyond VQA and RG, a spectrum of tasks contributes to the rich landscape of vision-language understanding [Che+23]. For instance, *referring expression comprehension* entails a model locating the specific area or object in an image that the given phrase or sentence refers to [ZNC18]. *Visual commonsense reasoning* involves answering questions about an image, typically presented in a multiple-choice format, and justifying the answer based on the model’s understanding of the image and common sense knowledge [Zel+19]. *Vision-language retrieval* focuses on either generating or retrieving relevant information from images using textual data, or vice versa, obtaining information from text using visual data [Zhe+19]. In the context of *visual captioning*, the model’s role is to generate a concise, text-based description of either an image [SDK23]. It is worth highlighting that some of these tasks can seamlessly transition from images to videos showcasing the adaptability and versatility of VLMs across diverse visual contexts [Gan+22].

Dataset	# image-text pairs	# QA pairs	Other components	Link
ROCO [Pel+18]	81,825	–	–	GH
MIMIC-CXR [Joh+19b]	377,110	–	–	PN
MIMIC-CXR-JPG [Joh+19a]	377,110	–	pathology labels	PN
MIMIC-NLE [Kay+22]	38,003	–	diagnosis labels, evidence labels	GH
CXR-PRO [RCR22]	–	–	374,139 reports, 374,139 radiographs	PN
MS-CXR [Boe+22]	1,162	–	bounding box annotations	PN
IU-Xray or OpenI [Dem+15]	7,470	–	labels	OpenI
MedICaT [Dem+15]	217,060, 7,507	–	annotations; inline references to ROCO figures	GH
PMC-OA [Lin+23a]	1,650,000	–	–	HF
SLAKE [Liu+21a]	–	14,028	642 annotated images, 5,232 medical triplets	MedVQA
VQA-RAD [Lau+18]	–	3,515	315 radiology images	Osf
PathVQA [He+20]	–	32,799	4,998 pathology images	GH
VQA-Med 2019 [Aba+19]	–	15,292	4,200 radiology images	GH
VQA-Med 2020 [Aba+20]	–	5,000	5,000 radiology images for VQA; images and questions for VQG	GH
VQA-Med 2021 [Ion+21]	–	5,500	5,500 radiology images for VQA; images and questions for VQG	GH
EndoVis 2017 [All+19]	–	472	bounding box annotations; 97 frames	GH
EndoVis 2018 [All+20]	–	11,783	bounding box annotations; 2,007 frames	GH challenge

Table 1: A list of medical vision-language datasets.

4 Medical Vision-Language Datasets

The adaptation of VLMs to the healthcare sector is achieved through their pre-training and fine-tuning using specialized medical datasets. Below is the list of vision-language datasets available to the public that contain medical image-text pairs or question-answer (QA) pairs. Most of them are employed by medical VLMs described in Section 6 for pre-training, fine-tuning, and evaluation of VQA and RG tasks. The comparative analysis of these datasets is presented in Table 1.

- *ROCO (Radiology Objects in Context)* [Pel+18] is a dataset composed of image-caption pairs extracted from the open-access biomedical literature database PubMed Central (PMC). ROCO is stratified into two categories: radiology and out-of-class. The radiology group includes 81,825 radiology images, including computer tomography (CT), ultrasound, x-ray, fluoroscopy, positron emission tomography (PET), mammography, magnetic resonance imaging (MRI), angiography, and PET-CT. The out-of-class group has 6,127 images, including synthetic radiology images, clinical photos, portraits, compound radiology images, and digital art. Each image is accompanied by a corresponding caption, keyword, Unified Medical Lan-

guage System (UMLS) semantic types (SemTypes), UMLS concept unique identifiers (CUIs), and a download link. To facilitate model training, the dataset is randomly split into a training set (65,460 radiology and 4,902 out-of-class images), a validation set (8,183 radiology and 612 out-of-class images), and a test set (8,182 radiology and 613 out-of-class images) using an 80/10/10 split ratio, respectively.

- *MIMIC-CXR* (*Medical Information Mart for Intensive Care - Chest X-Ray*) [Joh+19b] collection encompasses 377,110 chest X-rays paired with 227,835 associated free-text radiology reports. The dataset is derived from de-identified radiographic studies conducted at the Beth Israel Deaconess Medical Center in Boston, MA. Each imaging study within the MIMIC-CXR dataset consists of one or more images, typically featuring lateral and from back-to-front (posteroanterior, PA) views in Digital Imaging and Communications in Medicine (DICOM) format.
- *MIMIC-CXR-JPG* [Joh+19a] is a pre-processed variant of the MIMIC-CXR [Joh+19b] dataset. In this version, the original 377,110 images are converted into compressed JPG format. The 227,827 reports associated with these images are enriched with labels for various common pathologies. The labels are derived from the analysis of the impression, findings, or final sections of the radiology reports, facilitated by the use of NegBio [Pen+17] and CheXpert (Chest eXpert) [Irv+19] tools.
- *MIMIC-NLE* [Kay+22] dataset is specifically designed for the task of generating natural language explanations (NLEs) to justify predictions made on medical images, particularly in the context of thoracic pathologies and chest X-ray findings. The dataset consists of 38,003 image-NLE pairs or 44,935 image-diagnosis-NLE triplets, acknowledging instances where a single NLE may explain multiple diagnoses. NLEs are extracted from MIMIC-CXR [Joh+19b] radiology reports. The dataset exclusively considers X-ray views from front-to-back (anteroposterior, AP) and back-to-front (posteroanterior, PA). All NLEs come with diagnosis and evidence (for a diagnosis) labels. The dataset is split into the training set with 37,016 images, a test set with 273 images, and a validation set with 714 images.
- *CXR-PRO* (*CXR with Prior References Omitted*) [RCR22] dataset is derived from MIMIC-CXR [Joh+19b]. The dataset consists of 374,139 free-text radiology reports containing only the impression sections. It also incorporates associated chest radiographs; however, the radiology reports and chest X-rays are not paired. This dataset is designed to mitigate the problem of hallucinated references to prior reports often generated by radiology report generation ML models. The omission of prior references in this dataset aims to provide a cleaner and more reliable dataset for radiology RG.
- *IU-Xray* ((Indiana University chest X-rays) dataset, also known as the *Open-I* [Dem+15] dataset, is accessible through the National Library of Medicine’s Open-i service. The dataset originates from two hospital systems within the Indiana Network for Patient Care database. This dataset comprises 7,470 DICOM chest X-rays paired with 3,955 associated radiology reports. The reports typically include sections such as indications, findings, and impressions, and they are manually annotated using MeSH and RadLex (Radiology Lexicon) codes to represent clinical findings and diagnoses. Throughout this review, we will refer to the dataset interchangeably as *IU-Xray* and *Open-I*, maintaining consistency with the nomenclature used in related literature.

- *MedICaT (Medical Images, Captions, and Textual Reference)* [Sub+20] dataset contains 217,060 figures from 131,410 open-access PMC papers focused on radiology images and other medical imagery types. Excluding figures from ROCO [Pel+18], the dataset integrates inline references from the S2ORC (Semantic Scholar Open Research Corpus) [Lo+20] corpus, establishing connections between references and corresponding figures. Additionally, the inline references to ROCO figures are provided separately. MedICaT also contains 7,507 subcaption-subfigure pairs with annotations derived from 2,069 compound figures.
- *PMC-OA (PubMedCentral’s OpenAccess)* [Lin+23a] dataset comprises 1.65 M image-caption pairs, derived from PMC papers. It encompasses a variety of diagnostic procedures, including common ones such as ultrasound, MRI, PET, radioisotope, and rarer procedures like mitotic and fMRI. Additionally, the dataset covers a broad spectrum of diseases, with induced cataracts, ear diseases, and low vision being among the most frequently represented conditions.
- *MS-CXR* [Boe+22] dataset contains image bounding box labels paired with radiology findings, annotated and verified by two board-certified radiologists. The dataset consists of 1,162 image-text pairs of bounding boxes and corresponding text descriptions. The annotations cover 8 different cardiopulmonary radiological findings and are extracted from MIMIC-CXR [Joh+19b] and REFLACX (Reports and Eye-tracking data For Localization of Abnormalities in Chest X-rays) [Big+22] (based on MIMIC-CXR) datasets. The findings include atelectasis, cardiomegaly, consolidation, edema, lung opacity, pleural effusion, pneumonia, and pneumothorax.
- *SLAKE (Semantically-Labeled Knowledge-Enhanced)* is a English-Chinese bilingual dataset [Liu+21a]. It contains 642 images, including 12 diseases and 39 organs of the whole body. Each image is meticulously annotated with two types of visual information: masks for semantic segmentation and bounding boxes for object detection. The dataset includes a total of 14,028 QA pairs, categorized into vision-only or knowledge-based types and labeled accordingly, encompassing both open- and closed-ended questions. Moreover, SLAKE incorporates 5,232 medical knowledge triplets in the form of $\langle head, relation, tail \rangle$, where *head* and *tail* denote entities (e.g., organ, disease), and *relation* signify the relationship between these entities (e.g., function, treatment). An illustrative example of such a triplet is $\langle pneumonia, location, lung \rangle$.
- *VQA-RAD* [Lau+18] dataset contains 104 head axial single-slice CTs or MRIs, 107 chest x-rays, and 104 abdominal axial CTs. The images are meticulously chosen from MedPix, an open-access online medical image database, ensuring each image corresponds to a unique patient. Furthermore, every selected image has an associated caption and is deliberately devoid of any radiology markings. Every caption provides details about the imaging plane, modality, and findings generated and reviewed by expert radiologists. Also, VQA-RAD contains 3,515 QA pairs, with an average of 10 questions per image. Among them, 1,515 are free-form questions and answers, allowing for unrestricted inquiry. Additionally, 733 pairs involve rephrased questions and answers, introducing linguistic diversity. Another 1,267 pairs are framed, featuring questions presented in a structured format, offering consistency and systematic evaluation. Additionally, QA pairs are split into 637 open-ended and 878 closed-ended types. Within the closed-ended group, a predominant focus is on yes/no questions.
- *PathVQA* [He+20] is a dataset that encompasses 4,998 pathology images accompanied by a total of 32,799 QA pairs derived from these images. The images are sourced from pathology

books: “Textbook of Pathology” and “Basic Pathology”, and the digital library “Pathology Education Informational Resource”. Out of all QA pairs, 16,465 are of the open-ended type, while the remaining pairs are of the closed-ended yes/no type. On average, each image is associated with 6.6 questions, which cover a broad spectrum of visual contents, encompassing aspects such as color, location, appearance, shape, etc.

- *VQA-Med 2019* [Aba+19] dataset contains 4,200 radiology images obtained from MedPix, an open-access online medical image database, and 15,292 QA pairs. The training set consists of 3,200 images and 12,792 QA pairs, with each image having 3 to 4 associated questions. The validation set includes 500 images and 2,000 QA pairs, and the test set comprises 500 images and 500 QA pairs. The questions are mainly about modality, imaging plane, organ system, and abnormality.
- *VQA-Med 2020* [Aba+20] dataset contains 5,000 radiology images obtained from MedPix, an open-access online medical image database, and 5,000 QA pairs. The training set consists of 4,000 images and 4,000 QA pairs. The validation set comprises 500 images and 500 QA pairs, and the test set includes 500 images and 500 QA pairs. The questions are focused on abnormalities present in the images. Additionally, the dataset contains radiology images and questions for the Visual Question Generation (VQG) task. The training set consists of 780 images and 2,156 associated questions. The validation set comprises 141 images with 164 questions, and the test set includes 80 images.
- *VQA-Med 2021* [Ion+21] dataset contains 5,500 radiology images obtained from MedPix, an open-access online medical image database, and 5,500 QA pairs. The training set consists of 4,500 images and 4,500 QA pairs. The validation set comprises 500 images and 500 QA pairs, and the test set includes 500 images and 500 QA pairs. The questions are focused on abnormalities present in the images. Similarly to VQA-Med 2019, the dataset also contains radiology images and questions for the VQG task. The validation set comprises 85 images with 200 questions, and the test set includes 100 images.
- *EndoVis 2017* (Endoscopic Vision) [All+19] dataset contains 5 robotic surgery videos (two videos with 8 frames each, one with 18, one with 14, and one with 39 frames) from the MICCAI (Medical Image Computing and Computer Assisted Interventions) Endoscopic Vision 2017 Challenge. It also includes 472 QA pairs with bounding box annotations. These QA pairs are carefully crafted to involve specific inquiries related to the surgical procedure. Examples of questions include queries such as “What is the state of prograsp forceps?” and “Where is the large needle driver located?”. The inclusion of bounding box annotations enhances the dataset’s utility for tasks such as object detection or answer localization.
- *EndoVis 2018* [All+20] dataset contains 14 robotic surgery videos (2,007 frames in total) from the MICCAI Endoscopic Vision 2018 Challenge. It also includes 11,783 QA pairs regarding organs, surgical tools, and organ-tool interactions. When the question is about organ-tool interactions, the bounding box will contain both the organ and the tool.

5 Vision-Language Model Evaluation

This section delves into the evaluation process of medical VLMs. The initiation of this process involves meticulously selecting benchmark datasets and defining evaluation metrics tailored to the specific vision-language tasks at hand.

5.1 Evaluation Metrics for Report Generation

The prevalent benchmark datasets for medical RG are MIMIC-CXR [Joh+19b] and Open-I [Dem+15]. For more information on these datasets, see Section 4. Several metrics are used to evaluate the effectiveness of VLMs on RG tasks. The more frequently used metrics are outlined below.

- *BLEU (Bilingual Evaluation Understudy)* [Pap+02] score was originally designed for machine translation evaluation, but it has been adapted for RG and even VQA in a modified form. BLEU provides a quantitative measure of how well the machine-generated text aligns with human-generated reference text. First, the precision of different *n-grams*, which are consecutive sequences of n words, is calculated using the formula:

$$\text{Precision}(n) = \frac{\#\text{overlapping n-grams}}{\#\text{all n-grams in a model-generated text}}, \quad (1)$$

where *overlapping n-grams* refer to n-grams in the model-generated text that share common elements with at least one n-gram in the reference text. To ensure the precision score remains robust and is not disproportionately affected by repeated n-grams in the model-generated text, a modification known as *clipping* is often introduced. This process involves capping the count of each n-gram in the model-generated text to a maximum count. This maximum count is determined by the highest count observed in any single reference text for the same n-gram. The final *BLEU-n* score is defined as:

$$\text{BLEU-}n = \text{BP} \times \frac{1}{n} \exp \left(\sum_{k=1}^n \log(\text{Precision}(k)) \right),$$

where *BP* is a brevity penalty calculated as

$$\text{BP} = \begin{cases} 1 & \text{if } c \geq r \\ e^{(1-r/c)} & \text{if } c < r \end{cases}$$

where c is the length of the model-generated text, and r is the length of the reference text. It is common to use $n = 4$. The BLEU score ranges from 0 to 1, where a higher score suggests better agreement with the reference text. The overall BLUE score of the model is the average of BLUE scores for each pair of reports.

- *ROUGE (Recall-Oriented Understudy for Gisting Evaluation)* [Lin04] is a set of metrics that evaluate the overlap between the model-generated text and human-generated reference text. *ROUGE-n* assesses the overlap of n-grams between model-generated text and reference text, and it is defined as:

$$\text{ROUGE-}n = \frac{\#\text{overlapping n-grams}}{\#\text{all n-grams in a reference text}}.$$

ROUGE-L focuses on measuring the longest common subsequence between model-generated text Y and reference text X and it is calculated using the formula:

$$\text{ROUGE-L} = \frac{(1 + \beta^2) \times R \times P}{(R + P \times \beta^2)},$$

where $R = \frac{\text{LCS}(X,Y)}{m}$, $P = \frac{\text{LCS}(X,Y)}{n}$, m is the length of X , n is the length of Y , $\text{LCS}(X, Y)$ is the length of a longest common subsequence of X and Y , and β is a parameter that depends

on the specific task and the relative importance of precision (P) and recall (R). There are other ROUGE score variants. The ROUGE scores range from 0 to 1, where higher scores indicate similarity between the model-generated text and the reference text. For each ROUGE variant, the overall score of the model is the average of scores for each instance.

- *METEOR (Metric for Evaluation of Translation with Explicit ORdering)* [BL05] is an evaluation metric designed to be more forgiving than some other metrics and takes into account the fluency and meaning of the generated text. The METEOR score is computed as follows:

$$\text{METEOR} = \frac{10 \times P \times R}{R + 9 \times P} (1 - \text{Penalty}),$$

where

$$R = \frac{\#\text{overlapping 1-grams}}{\#\text{1-grams in a reference text}}, \quad P = \frac{\#\text{overlapping 1-grams}}{\#\text{1-grams in a model-generated text}},$$

$$\text{Penalty} = \frac{1}{2} \times \left(\frac{\#\text{chunks}}{\#\text{overlapping 1-grams}} \right)^3,$$

chunks are groups of adjacent 1-grams in the model-generated text that overlap with adjacent 1-grams in the reference text. The METEOR score ranges from 0 to 1, with higher scores indicating better alignment between the model-generated text and the reference text. The overall METEOR score of a model is the average of scores for each instance.

- *Perplexity* [Hao+20] measures the average uncertainty of a model in predicting each word in a text. The formula for perplexity is defined as:

$$\text{Perplexity} = e^{-\frac{1}{n} \sum_{k=1}^n \ln P(w_k | w_1, w_2, \dots, w_{k-1})},$$

where n is the total number of words in the text. The value of the perplexity metric can range from 1 to positive infinity, and lower values signify a more accurate and confident model in capturing the language patterns within the given text.

- *BERTScore* [Zha+20b] metric was initially designed for evaluating models that use **BERT** [Dev+19] embeddings. However, it can also leverage other word embeddings to evaluate the similarity between model-generated and reference text. The BERTScore of a single text pair is calculated according to the formula:

$$\text{BERTScore} = \frac{2 \times P \times R}{P + R},$$

where P represents the ratio of the maximum cosine similarity score between tokens in the model-generated text and the reference text to the numbers of tokens in the model-generated text and R represents the ratio of the maximum cosine similarity score between tokens in the model-generated text and the reference text to the numbers of tokens in the reference text. The BERTScore of the model is the average of BERTScores across all text pairs.

- *RadGraph F1* [Yu+23] is a novel metric that measures overlap in clinical entities and relations extracted from radiology reports. The RadGraph F1 score is computed in the following way. First, the **RadGraph** model maps model-generated and reference reports into graph representations with clinical entities represented as nodes and their relations as edges between them. Second, the number of nodes that match between the two graphs based on clinical

entity text and labels (entity type) is determined. Third, the number of edges that match between the two graphs based on their start and end entities and labels (relation type) is calculated. Lastly, the F1 score is separately computed for clinical entities and relations, and then the RadGraph F1 score for a report pair is the average of these two scores. The overall model performance is determined by averaging RadGraph F1 scores across all report pairs.

- *Human evaluation* plays a crucial role in assessing VLMS’s quality in medical RG. Human evaluation can be performed for RG in various ways. For instance, in [Jeo+23] expert radiologists evaluate the performance of the **X-REM** model in the RG task as follows. Initially, each report is segmented into lines, and radiologists assign scores to each line based on five error categories. These scores reflect the severity of errors, with higher values indicating more severe errors. Two metrics are utilized to obtain a comprehensive measure of the overall severity of errors in a report. *Maximum Error Severity (MES)* represents the highest score across all lines in the report, while *Average Error Severity (AES)* is calculated by averaging the scores across all lines in the report. According to radiologists, 18% of model-generated reports received an MES score of 0, while 24% received an AES score of 0.

The next few metrics are designed for classification evaluation, and RG can be viewed as such a task. In [Moo+22], [Lee+23], and [Pel+23], these metrics are computed based on the 14 labels obtained from applying the CheXpert [Irv+19] or CheXbert [Smi+20] labeler to the reference reports as well as the model-generated reports. In this context, reports bearing accurate diagnosis labels are categorized as positive, while those with inaccurate labels are regarded as negative. The following metrics are also called *clinical efficacy metrics*.

- *Accuracy* measures the ratio of all positive predictions to the total number of predictions.
- *Precision* is a metric that measures the accuracy of positive predictions made by a model. The precision score is calculated by considering the ratio of true positive predictions to the total number of instances that the model predicted as positive:

$$\text{Precision} = \frac{\text{True Positives}}{\text{True Positives} + \text{False Positives}}.$$

High precision indicates that the model has a low rate of false positives.

- *Recall* is a metric that assesses the ability of a model to predict all positive classes. Recall is defined as the ratio of correctly predicted positive observations to the total actual positives:

$$\text{Recall} = \frac{\text{True Positives}}{\text{True Positives} + \text{False Negatives}}.$$

The high recall means that the model effectively identifies most of the actual positive instances.

- *F1* metric assesses the overall model’s performance by balancing precision and recall into a single value. The F1 score is defined as:

$$F1 = \frac{2 \times \text{Precision} \times \text{Recall}}{\text{Precision} + \text{False Recall}}.$$

The F1 scores range from 0 to 1, with higher values indicating better performance. In multi-class classification, it is common to compute the *macro-F1* score by averaging the F1 scores calculated independently for each class. This method ensures an unbiased evaluation of the model’s performance across all classes, assigning equal importance to each class, irrespective of its size or prevalence in the dataset.

5.2 Evaluation Metrics for Visual Question Answering

The common benchmark datasets for medical VQA include VQA-RAD [Lau+18], SLAKE [Liu+21a], and PathVQA [He+20]. For more information on these datasets, see Section 4. Various metrics are available for VQA evaluation, and many of those used for RG can also be applied to VQA. To avoid redundancy with already mentioned metrics, only a few are highlighted below.

- *Accuracy* is a fundamental metric for gauging overall model correctness in VQA evaluation. It is determined by calculating the proportion of correctly predicted answers to the total number of questions. Sometimes, the *average accuracy* is computed by applying the model to various testing datasets, providing a comprehensive assessment of its performance across diverse scenarios.
- *Exact match* metric computes the ratio of generated answers that match exactly (excluding punctuation) the correct answer. However, this measure is rather strict, as it may not give credit to valuable answers that, despite being semantically correct, diverge from an exact lexical match with the correct answer. This metric is more suitable for evaluating answers to close-ended questions than open-ended ones.
- *Human evaluation* is valuable for assessing a model’s performance and applies not only to tasks such as VQA but also to RG. Human evaluation can be performed for VQA in various ways. For instance, in [Moo+23], the human evaluation process of **MedFlamingo** model employs an application featuring a user-friendly interface. Within this interface, medical experts are empowered to evaluate each VQA problem individually, assigning scores ranging from 0 to 10. The final scores of the few-shot performance are 5.61 on VQA-RAD, 1.81 on PathVQA, and 4.33 on the specifically curated Visual USMLE dataset. In contrast, the scores for zero-shot performance are lower, with 3.82 on RAD-VQA, 1.72 on PathVQA, and 4.18 on Visual USMLE.

6 Medical Vision-Language Models

This section presents an overview of existing medical VLMs tailored for visual question answering and/or report generation. The information is organized chronologically based on their first appearance. Our focus is mainly on models with available code, primarily those introduced more recently. A list of these VLMs is presented in Table 2.

- **MedViLL** (Medical Vision Language Learner) [Moo+22] is a VLM specifically developed for handling medical images and generating associated reports. It employs **ResNet-50** [He+16], trained on ImageNet [Den+09], for extracting visual feature vector \vec{v} . The model also leverages a base **BERT** [Dev+19] embedding layers to extract textual feature vectors \vec{t} from clinical reports, which are initially segmented into a sequence of tokens using a WordPiece [Wu+16] tokenizer. Both textual and visual features incorporate positional information to capture the spatial relationships and sequential order of elements in the input data. To generate a cross-modal representation, vectors \vec{v} and \vec{t} , along with special tokens [CLS] and [SEP], are concatenated as follows: $(\overrightarrow{CLS}, \vec{v}, \overrightarrow{SEP_V}, \vec{t}, \overrightarrow{SEP_L})$. The cross-modal representations are then fed into the BERT model. The MedViLL is pre-training on two tasks: MLM and ITM. The MLM task employs a *bidirectional auto-regressive (BAR)* self-attention mask, promoting the integration of image and language features. For MLM, a negative log-likelihood loss function

Model	Stream	Decoder	Architecture	VQA	RG	Datasets	Code
MedViLL [Moo+22]	single	No	RN50 + BERT	+	+	MIMIC-CXR, Open-I, VQA-RAD	GH
PubMedCLIP [EMD23]	dual	No	ViT-B/32 or RN50 or RN50×4 + Transformer + BAN	+	-	ROCO, SLAKE, VQA-RAD	GH
RepsNet [TBF22]	dual	No	ResNeXt-101 + BERT + BAN + GPT-2	+	+	VQA-RAD, IU-Xray	Site
BiomedCLIP [Zha+23b]	dual	No	ViT-B/16 + PubMedBERT + METER	+	-	PMC-15, SLAKE, VQA-RAD	HF
UniXGen [Lee+23]	single	No	VQGAN + Transformer	-	+	MIMIC-CXR	GH
RAMM [Yua+23]	dual	No	Swiss Transformer + PubMedBERT + multimodal encoder w/ retrieval-attention module	+	-	PMCPM, ROCO MIMIC-CXR, SLAKE, VQA-RAD, VQA-Med 2019, VQA-Med 2021	GH
X-REM [Jeo+23]	dual	No	ALBEF (ViT-B/16 + BERT + multimodal encoder)	-	+	MIMIC-CXR, MedNLI, RadNLI	GH
Visual Med-Alpaca [Shu+23]	single	No	DePlot or Med-GIT + prompt manager +LLaMa-7B	+	-	ROCO; MedDialog, MEDIQA QA, MEDIQA RQE, MedQA, PubMedQA + GPT-3.5-Turbo	GH
CXR-RePair-Gen [Ran+23b]	dual	No	ALBEF + FAISS retriever + prompt manager + text-davinci-003 or GPT-3.5-Turbo or GPT-4	-	+	CXR-PRO, MS-CXR	-
LLaVa-Med [Li+23a]	single	No	ViT-L/14 + projection layer + LLaMa-7B	+	-	PMC-15 + GPT-4, VQA-RAD, SLAKE, PathVQA	GH
XrayGPT [Tha+23]	single	No	MedCLIP + linear transformation layer + Vicuna-7B	+	+	MIMIC-CXR, Open-I	GH
CAT-ViL DeiT [BIR23]	single	No	RN18 + tokenizer + CAT-ViL fusion module + DeiT	+	-	EndoVis 2017, EndoVis 2018	GH
MUMC [Li+23b]	dual	Yes	ViT-B/12 + BERT + multimodal encoder + answer decoder	+	-	ROCO, MedICaT, ImageCLEF Caption, VQA-RAD, SLAKE PathVQA	GH
Med-Flamingo [Moo+23]	single	No	ViT-L/14 + perceiver resampler + LLaMa-7B	+	-	MTB, PMC-OA, VQA-RAD, PathVQA, Visual USMLE	GH
RaDialog [Pel+23]	single	No	BioViL-T + BERT + prompt manager + Vicuna-7B	+	+	MIMIC-CXR, Instruct	GH

Table 2: A list of medical VLMs designed for VQA and/or RG.

is used. The ITM task encourages learning visual and textual features by predicting matching pairs and employs a loss function based on predictions for matching and non-matching pairs. The model is pre-trained on 89,395 image-report pairs from the MIMIC-CXR [Joh+19b] dataset and then fine-tuned for downstream tasks on 3,547 pairs from the Open-I [Dem+15] dataset, an additional dataset comprising radiographic image-report pairs. Only AP view X-rays are included from both datasets for the analysis. VQA is performed on the VQA-RAD [Lau+18] dataset (see Table 3), including open and close-ended questions, where the output representation of [CLS] is used to predict a one-hot encoded answer. For radiology RG fine-tuning, the model uses *sequence-to-sequence (S2S)* mask instead of BAR and generates reports by sequentially recovering MASK tokens. RG is evaluated on MIMIC-CXR [Joh+19b] and Open-I [Dem+15]. MedViLL achieves a BLEU-4 score of 0.066, a perplexity value of 4.185, and using a CheXpert labeler [Irv+19] an accuracy of 84.1%, a precision value of 0.698, a recall value of 0.559, and an F1 score of 0.621 on MIMIC-CXR. Additionally, it achieves a BLEU-4 score of 0.049, a perplexity value of 5.637, an accuracy of 73.4%, a precision value of 0.512, a recall value of 0.594, and an F1 score of 0.550 on Open-I.

- **PubMedCLIP** [EMD23] is a **CLIP**-based [Rad+21] model pre-trained on ROCO [Pel+18] dataset, consisting of over 80K image-caption pairs sourced from PMC articles. The model utilizes CLIP text encoder, which is based on a Transformer [Vas+17] architecture, and three distinct CLIP visual encoders: **ViT-B/32** [Dos+21], **ResNet-50**, and **ResNet-50×4** [He+16]. Following the contrastive learning approach in CLIP, the model generates joint representations by computing cosine similarity between textual and visual features. The pre-training objective involves the computation of *cross-entropy loss* values for both vision and language. These losses are then averaged to derive an overall loss value. Following pre-training, the model is repurposed as a pre-trained visual encoder for VQA. The visual feature in VQA is the concatenation of the model’s output with the *convolutional denoising autoencoder (CDAE)* [Mas+11] output, an image denoising module. The question is encoded using a GloVe [PSM14] word embedding followed by an LSTM [HS97]. The image and question features are combined using *bilinear attention networks (BAN)* [KJZ18], and the resulting representations are passed through an answer classifier, which is a two-layer feed-forward NN. The VQA loss is determined by combining the classification and image reconstruction losses. During the VQA fine-tuning, the SLAKE (English) [Liu+21a] and VQA-RAD [Lau+18] datasets, comprising both open- and close-ended questions, are employed. The model’s effectiveness is evaluated in the context of two existing MedVQA (Medical Visual Question Answering) methods: MEVF (Mixture of Enhanced Visual Features) [Zha+20a] and QCR *question-conditioned reasoning (QCR)* [Liu+23a]. The assessment involved replacing the visual encoder component in MEVF and QCR with PubMedCLIP and subsequently evaluating the model’s performance. PubMedCLIP in the QCR framework achieves better accuracies on VQA-RAD and SLAKE datasets than in the MEVF framework. The highest accuracies of PubMedCLIP in the QCR framework on both datasets are shown in Table 3.
- **RepsNet** [TBF22] model is designed in a VQA setting and can generate automated medical reports and interpret medical images. It employs a modified version of the pre-trained **ResNeXt-101** [Xie+16] as its image encoder and utilizes pre-trained **BERT** [Dev+19] as the text encoder, with text tokenization done through WordPiece [Wu+16]. Fusion of image and question features is achieved using BAN [KJZ18]. To align images with textual descriptions, the model employs *bidirectional contrastive learning* [Che+20]. For VQA tasks, the model undergoes fine-tuning and evaluation on VQA-RAD [Lau+18] (see Table 3), while for

RG, fine-tuning and evaluation take place on IU-Xray [Dem+15] dataset. The model categorizes answers through classification for close-ended questions and generates answers using the modified version of **GPT-2** language decoder based on image features and prior context. The BLEU-2 and BLEU-4 scores of RepsNet on the IU-Xray dataset are 0.44 and 0.27, respectively.

- **BiomedCLIP** [Zha+23b] is pre-trained on the specifically curated PMC-15 dataset that consists of 15 M figure-caption pairs derived from the PMC articles, however, it is not publicly available. The model architecture is similar to **CLIP** [Rad+21], except that the text encoder is a pre-trained **PubMedBERT** [Gu+21] model with WordPiece tokenizer [Wu+16]. The model uses **ViT-B/16** [Dos+21] as the visual data encoder. During pre-training, the model adopts a contrastive learning approach, and to mitigate memory usage, it utilizes the *sharding contrastive loss* [Che+22]. For adaptation to VQA, the model incorporates the **METER** [Dou+22] framework. This involves deploying a *Transformer-based co-attention multimodal fusion module* that produces cross-modal representations. These representations are then fed into a classifier for the final prediction of answers. The model is evaluated on VQA-RAD [Lau+18] and SLAKE (English) [Liu+21a] datasets (see Table 3).
- **UniXGen** (Unified chest X-ray and report Generation model) [Lee+23] is a unified model that can generate both reports and view-specific X-rays. The model tokenizes chest X-rays leveraging **VQGAN** [ERO21], a generative model that amalgamates generative adversarial networks (GANs) with vector quantization (VQ) techniques. VQGAN employs an encoder to transform input images into continuous representations, subsequently using vector quantization to discretize them into learnable codebook vectors. Additionally, VQGAN incorporates a decoder, translating these discrete codes back into images during the generation process. For chest X-rays, multiple views from the same study are tokenized into sequences of discrete visual tokens, demarcated by special tokens to distinguish perspectives. In the case of radiology reports, the model uses a *byte-level BPE* [WCG20] tokenizer, augmented with sinusoid positional embedding for enhanced representation. The model is based on the Transformer architecture [Vas+17] with *multimodal causal attention mask*, ensuring that each position in the sequence attends to all previous positions and not future ones. During training, multiple views of chest X-rays and a report embedding are concatenated randomly and fed into the Transformer. The model is optimized using the negative log-likelihood loss function. The model is trained on 208,534 studies sampled from the MIMIC-CXR [Joh+19b] dataset. Each study contains at most three chest X-rays representing PA (from back to front), AP (from front to back), and lateral views. UniXGen achieves a BLEU-4 score of 0.050, and using a CheXpert labeler [Irv+19] a precision score of 0.431, a recall value of 0.410, and an F1 score of 0.420 on MIMIC-CXR dataset.
- **RAMM** (Retrieval-Augmented bioMedical Multi-modal pretrain-and-finetune paradigm) [Yua+23] is a retrieval-augmented VLM tailored for biomedical VQA. The model uses **Swin Transformer** [Liu+21b] as the image encoder and **PubMedBERT** [Gu+21] as the text encoder. The visual and textual features are then fused by the multimodal encoder, a 6-layer Transformer [Vas+17]. The model is pre-trained on the MIMIC-CXR [Joh+19b] and ROCO [Pel+18] datasets along with a newly curated dataset PMCPM (PMC-Patients-Multi-modal), consisting of 398,000 image-text pairs sampled from PMC-OA [Lin+23a] dataset. The model also employs contrastive learning, ITM and MLM and the pre-training objective function of the model is the sum of these three tasks. Using contrastive learning, the model aligns images and texts using the cosine similarity metric. The VQA task is viewed as a classification

problem and the model is optimized using the cross-entropy loss function. During model fine-tuning, a novel *retrieval-attention module* fuses the representations of the image-question input with 4 representations of the retrieved image-text pairs from the pre-trained datasets. This allows the model to focus on relevant parts of the retrieved information when generating answers. The model is evaluated on VQA-Med 2019 [Aba+19], VQA-Med 2021 [Ion+21], VQA-RAD [Lau+18], and SLAKE [Liu+21a] datasets (see Table 3).

- **X-REM** (Contrastive X-Ray REport Match) [Jeo+23] is a retrieval-based radiology RG model that uses an ITM score to measure the similarity of a chest X-ray image and radiology report for report retrieval. The VLM backbone of the model is **ALBEF** [Li+21]. ALBEF utilizes **ViT-B/16** [Dos+21] as its image encoder and initializes the text encoder with the first 6 layers of the **BERT** [Dev+19] base model. The *multimodal encoder* in ALBEF, responsible for combining visual and textual features to generate ITM scores, is initialized using the final six layers of the BERT base model. X-REM leverages ALBEF’s pre-trained weights and performs further pre-training on X-rays paired with extracted impression sections (2, 192 pairs), findings sections (1, 597 pairs), or both (2, 192 pairs) from the MIMIC-CXR [Joh+19b] dataset. Subsequently, the model is fine-tuned on the ITM task, where the scoring mechanism involves using the logit value for the positive class as the similarity score for image-text pairs. To address the positive skewness in medical datasets, 14 clinical labels obtained from the CheXbert [Smi+20] labeler are utilized. The model efficiently manages the computational burden associated with ITM scores by employing ALBEF’s pre-aligned unimodal embeddings. This involves narrowing down the candidate reports based on high cosine similarity with the input image before computing ITM scores. Additionally, the text encoder undergoes fine-tuning on *natural language inference (NLI)* task, utilizing datasets such as MedNLI [RS18] and RadNLI [Miu+21]. This step is crucial for preventing the retrieval of multiple reports with overlapping or conflicting information. X-REM achieves a BLUE-2 score of 0.186 on the MIMIC-CXR (Findings only) dataset. The BERTScore of the model is 0.386 on MIMIC-CXR (Findings only) and is 0.287 on MIMIC-CXR (Impressions and Findings). The human evaluation of X-REM is described in Section 5.
- **Visual Med-Alpaca** [Shu+23] is a biomedical foundational model designed for addressing multimodal biomedical tasks like VQA. The model is constructed in the following way. First, image inputs go through a classifier to determine the appropriate module for transforming visual information into an intermediate text format. The currently supported modules include **DePlot** [Liu+22], utilized for interpreting plots and charts, and **Med-GIT** [Wan+22a], fine-tuned specifically on the ROCO [Pel+18] dataset for understanding radiology images. The prompt manager then amalgamates textual information extracted from images and text inputs to construct the prompt for the LLM model, **LLaMA-7B** [Tou+23b]. However, before generating responses, LLaMa-7B undergoes both standard fine-tuning and LoRA [Hu+22] fine-tuning on a carefully curated set of 54,000 medical question-answer pairs. The questions within this set are derived from question answering datasets such as MEDIQA QA [BSD19], MEDIQA RQE [BSD19], MedQA [Jin+21], MedDialog [Zen+20], and PubMedQA [Jin+19], with their corresponding answers synthesized using **GPT-3.5-Turbo** in the *self-instruct* [Wan+23b] manner. Human experts then meticulously filter and edit the obtained question-answer pairs to ensure quality and relevance. The evaluation of this model is still ongoing.
- **CXR-RePaiR-Gen** (Contrastive X-ray-Report Pair Retrieval based Generation) [Ran+23b] is a VLM designed for radiology RG that incorporates the RAG framework to mitigate the

issue of *hallucinated references* in RG. The model leverages the pre-trained **ALBEF** [Lan+19] previously utilized in the **CXR-ReDone** [RCR22] model. The ALBEF model consists of a **ViT-B/16** [Dos+21] image encoder and the first 6 layers of **BERT** [Dev+19] as the text encoder, producing contrastively aligned image and text embeddings. Textual features are indexed in a vector database FAISS (Facebook AI Similarity Search), and when given a radiology image input, embeddings from the reports or sentences corpus with the highest dot-product similarity to the image embedding are retrieved. The CXR-PRO [RCR22] dataset is employed for text retrieval to gather relevant impressions for generating the radiology report. The retrieved impression sections from the CXR-PRO dataset serve as the context for the prompt to an LLM, along with instructions to generate the radiology report. Two distinct prompts are employed for generating free-text reports: one for the **text-davinci-003** model and another for RG in a conversational setting with the **GPT-3.5-Turbo** and **GPT-4** models. The model is evaluated on MS-CXR [Boe+22] and CXR-PRO datasets. There is no code provided for this model yet. CXR-RePaiR-Gen reaches a BERTScore score of 0.2865 on the CXR-PRO dataset when based on **GPT-4**. Additionally, **CXR-RePaiR-Gen** achieves a score of 0.1970 on MS-CXR when based on **text-davinci-003**. The model attains a RadGraph F1 score of 0.1061 on the CXR-PRO dataset when based on **GPT-4** and 0.0617 on the MS-CXR dataset when it is based on **text-davinci-003**. In these instances, the CXR-RePaiR-Gen utilizes three retrieval samples per input during the RAG process.

- **LLaVa-Med** (Large Language and Vision Assistant for BioMedicine) [Li+23a] is an adaptation of the VLM **LLaVa** [Liu+23b], specifically tailored for the medical domain through training on instruction-following datasets. The visual features are generated by the pre-trained **CLIP** ([Rad+21]) visual encoder **ViT-L/14** [Dos+21]. The encoder can be substituted with **BiomedCLIP** [Zha+23b]. These features are passed through a linear projection layer, which converts them into tokens, and then, together with the tokenized instructions, are fed into the LLM **LLaMa-7B** [Tou+23b]. The LLM can be substituted with **Vicuna** [Chi+23]. After being initialized with the general-domain LLava, the model undergoes fine-tuning using curriculum learning. First, the model tries to understand and connect visual elements in biomedical images to the corresponding words or descriptions in the language model’s knowledge. To achieve that, a dataset consisting of 600,000 image-caption pairs from the PMC-15 dataset, which was originally employed in the training of BiomedCLIP, is utilized. These image-caption pairs are transformed into an instruction-following dataset, where the instructions prompt the model to describe the corresponding image concisely or in detail. Given the language instruction and image input, the model is then prompted to predict the original caption. During this stage, the visual encoder and language model weights are kept frozen, with updates exclusively applied to the linear projection layer. The second stage of training focuses on aligning the model to follow diverse instructions. For this purpose, another instruction-following dataset is generated from PMC-15. For this dataset, instructions are designed to guide **GPT-4** to generate multi-round questions and answers from the image caption and sentences from the original PMC paper that mentions the image [Li+23a]. In this training phase, the model undergoes training on a set of 60,000 images, each accompanied by its respective caption and multi-round questions and answers. Throughout this process, the weights of the visual encoder remain unchanged, preserving the previously acquired visual features. Meanwhile, the pre-trained weights of both the projection layer and the language model undergo continuous updates. This approach enables the model to effectively respond to a variety of instructions and perform well in generating dynamic and informative multi-round conversational content. Lastly, for VQA the model is fine-tuned and evaluated on VQA-RAD

[Lau+18], SLAKE [Liu+21a], and PathVQA [He+20] (see Table 3).

- **XrayGPT** [Tha+23] is a conversational medical VLM specifically developed for analyzing chest radiographs. It uses **MedCLIP** [Wan+22b] as a vision encoder to generate visual features. These features undergo a meticulous transformation process: initially, they are mapped to a lower-dimensional space through a linear projection head and subsequently translated into tokens via a linear transformation layer. At its core, the model incorporates two text queries. The Assistant query plays a role in contextualizing the model’s behavior and defining its purpose as “You are a helpful healthcare virtual assistant”. The Doctor’s query serves as a prompt that guides the model in providing information relevant to chest X-ray analysis. Tokens generated from a visual input are concatenated with the tokenized queries and then fed into the medical LLM, which generates the summary of the chest x-ray. The LLM employed in this architecture is **Vicuna-7B** [Chi+23], fine-tuned on a rich dataset consisting of 100,000 real conversations between patients and doctors, along with 20,000 radiology conversations sourced from ShareGPT.com. During training, both the vision encoder and the LLM remain frozen, while the weights in the linear transformation layer undergo updates. The model is first trained on 213,514 image-text pairs from pre-processed MIMIC-CXR [Joh+19b] dataset and then on 3,000 image-text pairs from Open-I [Dem+15] dataset. XrayGPT achieves ROUGE-1 = 0.3213, ROUGE-2 = 0.0912, and ROUGE-L = 0.1997 on MIMIC-CXR dataset.
- **CAT-ViL DeiT** [BIR23] stands out as a specialized medical Vision-Language Model (VLM) tailored for Visual Question Answering (VQA) within surgical scenarios, with a unique focus on answer localization. The architecture incorporates a **ResNet-18** [He+16] as the visual encoder, pre-trained on ImageNet [Den+09], and a customized pre-trained **BERT** tokenizer [See+22] for the text encoder. Central to its functionality is the *Co-Attention gaTed Vision-Language (CAT-ViL) module*, which enables interaction between visual and textual features and fuses them via a gating mechanism to obtain optimized multimodal embeddings. These features are then fused using a gating mechanism, yielding optimized multimodal embeddings. The model further integrates a pre-trained *Data-efficient image Transformer (DeiT)* [Tou+21] module to process these multimodal embeddings, aiming to acquire an optimal joint representation for comprehensive visual and textual understanding. In the context of VQA, the model adopts a standard classification head, while for answer localization within images, it employs the *detection with transformers (DETR)* [Car+20] head. The overall loss function comprises cross-entropy as the classification loss and L1-norm, along with the *generalized intersection over union (GIoU)* [Rez+19], serving as the localization loss. The model is trained on 1,560 frames and 9,014 QA pairs from the surgical datasets EndoVis 2018 [All+20]. The model achieved an accuracy of 61.92% on the remaining data from EndoVis 2018 and 45.55% on EndoVis 2017 [All+19] dataset.
- **MUMC** (Masked image and text modeling with Unimodal and Multimodal Contrastive losses) [Li+23b] is a VLM designed for medical VQA. The model utilizes a ViT-B/12 [Dos+21] as its image encoder, the first 6 layers of BERT [Dev+19] as its text encoder, and the last 6 layers of BERT as its multimodal encoder. The multimodal encoder incorporates cross-attention layers to align visual and textual features. For pre-training, the model employs a combination of contrastive learning, MLM, and ITM objectives. Also, the model utilizes a newly introduced *masked image strategy*, randomly masking 25% of image patches as a data augmentation technique. This exposes the model to a greater variety of visual contexts and enables learning representations that are more robust to partially occluded inputs. The pre-

training is performed on the ROCO [Rad+21], MedICaT [Sub+20], and ImageCLEF (Image Retrieval in Cross-Language Evaluation Forum) Caption [Rüc+22] datasets. For downstream VQA tasks, an answering decoder is added on top of the multimodal encoder to generate answer text tokens. The encoder weights are initialized from pre-training, and the model is fine-tuned and evaluated on VQA-RAD [Lau+18], SLAKE [Liu+21a], and PathVQA [He+20] (see Table 3).

- **Med-Flamingo** [Moo+23] is a multimodal *few-shot learner* model based on the **Flamingo** [Ala+22] architecture, adapted to medical domain. The model is pre-trained on the MTB [Moo+23] dataset, a newly curated collection comprising 4,721 segments from various Medical TextBooks, encompassing both textual content and images. Each segment is designed to contain at least one image and up to 10 images, with a specified maximum length. Also, it is pre-trained on 1.3 M image-caption pairs from the PMC-OA [Lin+23a] dataset. The Model’s few-shot capabilities are achieved through training on these mixed text and image datasets, enabling it to generalize and perform diverse multimodal tasks with only a few examples. The model utilizes pre-trained frozen **CLIP** vision encoder **ViT-L/14** for visual features generation. To convert these visual features into a fixed number of tokens, the model employs a module known as the *perceiver resampler*, which is trained from scratch. Subsequently, these tokens, along with tokenized text inputs, undergo further processing in a pre-trained frozen LLM **LLaMA-7B** [Tou+23b], enhanced with strategically inserted *gated cross-attention layers* that are also trained from scratch. This augmentation not only facilitates the learning of novel relationships but also bolsters training stability. The model’s performance is evaluated on established benchmarks such as VQA-RAD [Lau+18] and PathVQA [He+20], demonstrating its effectiveness in medical visual question-answering. The exact match scores for MedFlamingo demonstrate a few-shot performance of 0.200 on VQA-RAD and 0.303 on PathVQA. In contrast, the zero-shot performance yields an exact match score of 0.000 on VQA-RAD and 0.120 on PathVQA. Additionally, it is evaluated on a specifically created Visual USMLE (United States Medical Licensing Examination) dataset, comprising 618 challenging open-ended USMLE-style questions augmented with images, case vignettes, and tables of laboratory measurements, covering a diverse range of medical specialties. The human evaluation of the MedFlamingo model on VQA-RAD, PathVQA, and Visual USMLE datasets is described in Section 5.
- **RaDialog** [Pel+23] is a VLM that integrates automated radiology RG with conversational assistance. The model incorporates **BioViL-T** [Ban+23], a hybrid model that amalgamates the strengths of **ResNet-50** [He+16] and Transformer [Vas+17] architectures. Pre-trained on radiology images and reports, BioViL-T serves as a vision encoder that generates patch-wise visual features. The extracted features undergo alignment through a **BERT** [Dev+19] model, transforming them into a concise representation of 32 tokens. The model incorporates the CheXpert classifier to offer organized findings in medical images. These findings are generated based on labels obtained from the CheXbert [Smi+20] model. The classifier is trained independently using labels predicted by CheXbert from the findings section of radiology reports. The model integrates visual features, structured findings, and the directive “Write a radiology report” into a singular prompt, which is used as input for the LLM, a **Vicuna-7B** [Chi+23] model fine-tuned using LoRA [Hu+22]. The training is performed on X-ray image-report pairs from MIMIC-CXR [Joh+19b] dataset. RaDialog achieves a BLUE-4 score of 0.095, ROUGE-L score of 0.2710, METEOR score of 0.14, and BERTScore of 0.400 on the MIMIC-CXR dataset. To address the challenge of *catastrophic forgetting* during training and

Model	SLAKE		VQA-RAD		PathVQA		VQA-Med 2019	VQA-Med 2021
	open-ended	close-ended	open-ended	close-ended	open-ended	close-ended		
MedViLL [Moo+22]	–	–	59.50%	77.70%	–	–	–	–
PubMedCLIP [EMD23]	78.40%	82.50%	60.10%	80.00%	–	–	–	–
RepsNet [TBF22]	–	–	–	<u>87.05%</u>	–	–	–	–
BioMedCLIP [Zha+23b]	<u>82.50%</u>	89.70%	67.60%	79.80%	–	–	–	–
RAMM [Yua+23]	82.48%	<u>91.59%</u>	67.60%	85.29%	–	–	<u>82.13%</u>	<u>39.20%</u>
LLaVa-Med [Li+23a]	–	84.19%	–	85.34%	–	<u>91.21%</u>	–	–
MUMC [Li+23b]	–	–	71.50%	84.20%	<u>39.00%</u>	90.4%	–	–

Table 3: The comparison of medical VLMs’ accuracies on VQA tasks. The underlined accuracies are the highest for a specific dataset.

ensure the model’s capability across diverse downstream tasks, it is specifically trained on the newly created Instruct [Pel+23] dataset. This dataset is meticulously curated to encompass a spectrum of 8 diverse tasks: RG, NLE, complete CheXpert QA, binary CheXpert QA, region QA, summarization, report correction, and reformulation report using simple language. Each task is accompanied by carefully formulated prompts, tailored to elicit specific responses from the model. For instance, some prompts involve answering questions about particular X-ray regions. RaDialog trained on the Instruct dataset achieves an F1 score of 0.397 on the binary CheXpert QA task and 0.403 on the complete CheXpert QA task while RaDialog without being trained on Instruct achieves lower F1 scores of 0.018 and 0.098, respectively.

7 Challenges & Future Directions

In medical AI, the future holds great promise and, concurrently, poses notable challenges [Aco+22]. As technology advances, the integration of VLMs into the healthcare sector has the potential to revolutionize diagnostics, treatment planning, and patient care. Future medical VLMs may offer enhanced capabilities in understanding complex clinical scenarios, generating detailed reports of medical images, and facilitating seamless communication between healthcare professionals and AI systems. However, these advancements come with challenges.

A significant challenge in developing effective medical VLMs is the lack of diverse and representative medical datasets. This limitation restricts the comprehensive training of VLMs, impeding their ability to understand the complexities of diverse and rare clinical scenarios [Moo+23]. Retrieval-augmented generation (RAG) presents a potential solution by enhancing training datasets through incorporation of retrieved relevant information. While RAG usually involves a frozen model during training, exploring the pre-training of VLMs within the RAG framework opens up a new avenue of research [Zha+23d]. This innovative approach could potentially enhance the robustness of VLMs, especially in handling new and unforeseen medical cases.

Traditional metrics may fall short in capturing the nuanced complexities of clinical language, posing a barrier to reliable evaluations of VLM performance [Yu+23]. This issue becomes partic-

ularly evident when evaluating the accuracy of medical reports or addressing open-ended medical queries, where metrics need to discern clinically relevant distinctions. Therefore, development and adoption of specialized metrics tailored for medical RG and VQA become imperative. Such metrics are pivotal not only for evaluating model performance but also for assessing aspects like generalization, efficiency, and robustness. The establishment of these metrics will significantly contribute to fostering precise evaluations and continual advancements in the capabilities of medical VLMs.

The issue of *hallucinations* in VLMs poses a significant challenge to their reliability and practical application [Liu+24]. Hallucinations refer to instances where VLMs generate outputs that are not grounded in the provided images, or are inconsistent with the established knowledge. In medical contexts, these hallucinations can have serious consequences, leading to inaccurate diagnostic information or treatment recommendations. One identified root cause of hallucinations is the lack of alignment between visual and textual modalities [Sun+23]. Training VLMs to effectively align these modalities is crucial in mitigating the risk of hallucinations. For instance, **LLaVA-RLHF** [Sun+23] achieved hallucination reduction by incorporating RLHF to align different modalities.

Overcoming *catastrophic forgetting* poses an additional challenge in the development of medical VLMs. Catastrophic forgetting occurs when a model learning new information inadvertently erases or distorts previously acquired knowledge, potentially compromising its overall competence. Striking a balance during fine-tuning can be crucial; moderate fine-tuning can be helpful to adapt the model to a specific task, while excessive fine-tuning can lead to catastrophic forgetting [Zha+23a]. Leveraging methodologies from *continual learning* [Wan+23a; Zho+23b; CR24] might be useful in the context of medical VLMs, where the ability to adapt and accumulate knowledge across diverse clinical tasks is paramount. Continual learning focuses on training models to sequentially learn from and adapt to new data over time while retaining knowledge from previously encountered tasks. Also, incorporating adapters within the framework of continual learning can be a valuable tool in mitigating catastrophic forgetting [Zha+23c].

Finally, clinical validation and adoption of VLMs necessitate a collaborative bridge between medical experts and machine learning researchers. Trust, alignment with clinical needs, and ethical deployment are critical components for the successful integration of these models into healthcare workflows. Establishing robust collaborations ensures a dynamic synergy, combining domain expertise with technological advancements. This synergy is essential for the responsible and effective deployment of medical VLMs in healthcare.

References

[Aba+20] Asma Ben Abacha et al. “Overview of the VQA-Med Task at ImageCLEF 2020: Visual Question Answering and Generation in the Medical Domain”. In: *CLEF 2020 Working Notes*. CEUR Workshop Proceedings. 2020.

[Aba+19] Asma Ben Abacha et al. “VQA-Med: Overview of the Medical Visual Question Answering Task at ImageCLEF 2019”. In: *Conference and Labs of the Evaluation Forum*. 2019. URL: <https://api.semanticscholar.org/CorpusID:198489641>.

[Aco+22] Julián N Acosta et al. “Multimodal Biomedical AI”. In: *Nature Medicine* 28.9 (2022), pp. 1773–1784.

[Ala+22] Jean-Baptiste Alayrac et al. “Flamingo: A Visual Language Model for Few-Shot Learning”. In: *Advances in Neural Information Processing Systems*. 2022. URL: <https://api.semanticscholar.org/CorpusID:248476411>.

[All+19] Max Allan et al. *2017 Robotic Instrument Segmentation Challenge*. 2019. arXiv: 1902.06426.

[All+20] Max Allan et al. *2018 Robotic Scene Segmentation Challenge*. 2020. arXiv: 2001.11190.

[Ant+15] Stanislaw Antol et al. “VQA: Visual Question Answering”. In: *IEEE International Conference on Computer Vision (ICCV)*. 2015, pp. 2425–2433. DOI: 10.1109/ICCV.2015.279.

[Bai+23] Jinze Bai et al. *Qwen-VL: A Versatile Vision-Language Model for Understanding, Localization, Text Reading, and Beyond*. 2023. arXiv: 2308.12966.

[BIR23] Long Bai, Mobarakol Islam, and Hongliang Ren. “CAT-ViL: Co-attention Gated Vision-Language Embedding for Visual Question Localized-Answering in Robotic Surgery”. In: *Medical Image Computing and Computer Assisted Intervention – MICCAI*. 2023, pp. 397–407.

[Baj+21] Junaid Bajwa et al. “Artificial Intelligence in Healthcare: Transforming the Practice of Medicine”. In: *Future Healthcare Journal* 8.2 (2021), e188–e194. DOI: 10.7861/fhj.2021-0095.

[Bal21] Pierre Baldi. *Deep Learning in Science*. Cambridge University Press, 2021.

[BL05] Satanjeev Banerjee and Alon Lavie. “METEOR: An Automatic Metric for MT Evaluation with Improved Correlation with Human Judgments”. In: *ACL Workshop on Intrinsic and Extrinsic Evaluation Measures for Machine Translation and/or Summarization*. 2005, pp. 65–72. URL: <https://www.aclweb.org/anthology/W05-0909>.

[Ban+23] Shruthi Bannur et al. *Learning to Exploit Temporal Structure for Biomedical Vision-Language Processing*. 2023. arXiv: 2301.04558.

[Baz+23] Yakoub Bazi et al. “Vision–Language Model for Visual Question Answering in Medical Imagery”. In: *Bioengineering* 10.3 (2023). URL: <https://doi.org/10.3390/bioengineering10030380>.

[Bea+20] Andrew Beam et al. “Clinical Concept Embeddings Learned from Massive Sources of Multimodal Medical Data”. In: *Pacific Symposium on Biocomputing. Pacific Symposium on Biocomputing* 25 (2020), pp. 295–306.

[BSD19] Asma Ben Abacha, Chaitanya Shivade, and Dina Demner-Fushman. “Overview of the MEDIQA 2019 Shared Task on Textual Inference, Question Entailment and Question Answering”. In: *BioNLP Workshop and Shared Task*. 2019, pp. 370–379. DOI: 10.18653/v1/W19-5039. URL: <https://aclanthology.org/W19-5039>.

[Big+22] Ricardo Bigolin Lanfredi et al. “REFLACX, a Dataset of Reports and Eye-tracking Data for Localization of Abnormalities in Chest X-rays”. In: *Scientific Data* 9.1 (2022). DOI: 10.1038/s41597-022-01441-z. URL: <http://dx.doi.org/10.1038/s41597-022-01441-z>.

[Boe+22] Benedikt Boecking et al. “Making the Most of Text Semantics to Improve Biomedical Vision–Language Processing”. In: *Computer Vision – ECCV*. 2022, pp. 1–21. DOI: https://doi.org/10.1007/978-3-031-20059-5_1.

[Boe+21] Kevin Michael Boehm et al. “Harnessing Multimodal Data Integration to Advance Precision Oncology”. In: *Nature Reviews Cancer* 22 (2021), pp. 114–126. URL: <https://www.nature.com/articles/s41568-021-00408-3>.

[Boj+17] Piotr Bojanowski et al. “Enriching Word Vectors with Subword Information”. In: *Transactions of the Association for Computational Linguistics* 5 (2017), pp. 135–146. ISSN: 2307-387X.

[Bro+20] Tom B. Brown et al. “Language Models are Few-Shot Learners”. In: *Advances in Neural Information Processing Systems*. Vol. 33. 2020.

[CR24] Yuliang Cai and Mohammad Rostami. *Dynamic Transformer Architecture for Continual Learning of Multimodal Tasks*. 2024. arXiv: 2401.15275.

[Car+20] Nicolas Carion et al. “End-to-End Object Detection with Transformers”. In: *European conference on computer vision*. 2020, pp. 213–229.

[Che+23] Feilong Chen et al. “VLP: A Survey on Vision-Language Pre-Training”. In: *Machine Intelligence Research* 20 (2023), pp. 38–56.

[Che+20] Ting Chen et al. *A Simple Framework for Contrastive Learning of Visual Representations*. 2020. arXiv: 2002.05709.

[Che+19] Yen-Chun Chen et al. “UNITER: UNiversal Image-TExt Representation Learning”. In: *European Conference on Computer Vision*. 2019. URL: <https://api.semanticscholar.org/CorpusID:216080982>.

[Che+22] Mehdi Cherti et al. *Reproducible Scaling Laws for Contrastive Language-Image Learning*. 2022. arXiv: 2212.07143.

[Chi+23] Wei-Lin Chiang et al. *Vicuna: An Open-Source Chatbot Impressing GPT-4 with 90%* ChatGPT Quality*. 2023. URL: <https://lmsys.org/blog/2023-03-30-vicuna/>.

[Cho+21] Jaemin Cho et al. “Unifying Vision-and-Language Tasks via Text Generation”. In: *International Conference on Machine Learning*. 2021. URL: <https://proceedings.mlr.press/v139/cho21a.html>.

[Cho+14] Kyunghyun Cho et al. “Learning Phrase Representations using RNN Encoder–Decoder for Statistical Machine Translation”. In: *Conference on Empirical Methods in Natural Language Processing*. 2014. URL: <https://api.semanticscholar.org/CorpusID:5590763>.

[Cho+22] Aakanksha Chowdhery et al. “PaLM: Scaling Language Modeling with Pathways”. In: *Journal of Machine Learning Research* 24 (2022), 240:1–240:113. URL: <https://api.semanticscholar.org/CorpusID:247951931>.

[Dai+23] Wenliang Dai et al. *InstructBLIP: Towards General-purpose Vision-Language Models with Instruction Tuning*. 2023. arXiv: 2305.06500.

[Dao23] Tri Dao. *FlashAttention-2: Faster Attention with Better Parallelism and Work Partitioning*. 2023. arXiv: 2307.08691.

[Dem+15] Dina Demner-Fushman et al. “Preparing a Collection of Radiology Examinations for Distribution and Retrieval”. In: *Journal of the American Medical Informatics Association (JAMIA)* 23 2 (2015), pp. 304–10. URL: <https://api.semanticscholar.org/CorpusID:16941525>.

[Den+09] Jia Deng et al. “ImageNet: A Large-Scale Hierarchical Image Database”. In: *2009 IEEE Conference on Computer Vision and Pattern Recognition*. 2009, pp. 248–255. DOI: 10.1109/CVPR.2009.5206848.

[Dev+19] Jacob Devlin et al. “BERT: Pre-Training of Deep Bidirectional Transformers for Language Understanding”. In: *Conference of the North American Chapter of the Association for Computational Linguistics*. Vol. 1. 2019. doi: 10.18653/v1/N19-1423.

[Dos+21] Alexey Dosovitskiy et al. “An Image is Worth 16x16 Words: Transformers for Image Recognition at Scale”. In: *International Conference on Learning Representations*. 2021. URL: <https://openreview.net/forum?id=YicbFdNTTy>.

[Dou+22] Zi-Yi Dou et al. “An Empirical Study of Training End-to-End Vision-and-Language Transformers”. In: *IEEE/CVF Conference on Computer Vision and Pattern Recognition (CVPR)*. 2022, pp. 18145–18155. DOI: 10.1109/CVPR52688.2022.01763.

[EMD23] Sedigheh Eslami, Christoph Meinel, and Gerard De Melo. “PubMedCLIP: How Much Does CLIP Benefit Visual Question Answering in the Medical Domain?” In: *Findings of the Association for Computational Linguistics*. 2023, pp. 1151–1163.

[ERO21] Patrick Esser, Robin Rombach, and Björn Ommer. “Taming Transformers for High-Resolution Image Synthesis”. In: *2021 IEEE/CVF Conference on Computer Vision and Pattern Recognition (CVPR)*. 2021, pp. 12868–12878. DOI: 10.1109/CVPR46437.2021.01268. URL: <https://doi.ieee.org/10.1109/CVPR46437.2021.01268>.

[Gan+22] Zhe Gan et al. *Vision-Language Pre-training: Basics, Recent Advances, and Future Trends*. 2022. arXiv: 2210.09263.

[Gir+14] Ross B. Girshick et al. “Rich Feature Hierarchies for Accurate Object Detection and Semantic Segmentation”. In: *IEEE Conference on Computer Vision and Pattern Recognition*. 2014, pp. 580–587. URL: <https://api.semanticscholar.org/CorpusID:215827080>.

[Gu+23] Jindong Gu et al. *A Systematic Survey of Prompt Engineering on Vision-Language Foundation Models*. 2023. arXiv: 2307.12980.

[Gu+21] Yu Gu et al. “Domain-Specific Language Model Pretraining for Biomedical Natural Language Processing”. In: *ACM Transactions on Computing for Healthcare* 3.1 (2021), p. 23. DOI: 10.1145/3458754. URL: <https://doi.org/10.1145/3458754>.

[Han+23] Tianyu Han et al. *MedAlpaca – An Open-Source Collection of Medical Conversational AI Models and Training Data*. 2023. arXiv: 2304.08247.

[Hao+20] Yiding Hao et al. *Probabilistic Predictions of People Perusing: Evaluating Metrics of Language Model Performance for Psycholinguistic Modeling*. 2020. arXiv: 2009.03954.

[He+23] Kai He et al. *A Survey of Large Language Models for Healthcare: from Data, Technology, and Applications to Accountability and Ethics*. 2023. arXiv: 2310.05694.

[He+16] Kaiming He et al. “Deep Residual Learning for Image Recognition”. In: *IEEE Conference on Computer Vision and Pattern Recognition*. 2016, pp. 770–778. DOI: 10.1109/CVPR.2016.90.

[He+17] Kaiming He et al. “Mask R-CNN”. In: *IEEE International Conference on Computer Vision (ICCV)*. 2017, pp. 2980–2988. DOI: 10.1109/ICCV.2017.322.

[He+20] Xuehai He et al. *PathVQA: 30000+ Questions for Medical Visual Question Answering*. 2020. arXiv: 2003.10286.

[HS97] Sepp Hochreiter and Jürgen Schmidhuber. “Long Short-Term Memory”. In: *Neural Computation* 9.8 (1997), pp. 1735–1780. DOI: 10.1162/neco.1997.9.8.1735. URL: <https://doi.org/10.1162/neco.1997.9.8.1735>.

[Hu+22] Edward J Hu et al. “LoRA: Low-Rank Adaptation of Large Language Models”. In: *International Conference on Learning Representations*. 2022. URL: <https://openreview.net/forum?id=nZeVKeeFYf9>.

[Hua+19] Gao Huang et al. “Convolutional Networks with Dense Connectivity”. In: *IEEE Transactions on Pattern Analysis and Machine Intelligence* (2019).

[Hua+21] Yu Huang et al. “What Makes Multimodal Learning Better than Single (Provably)”. In: *Advances in Neural Information Processing Systems*. 2021. URL: <https://api.semanticscholar.org/CorpusID:235367766>.

[Ion+21] Bogdan Ionescu et al. “Overview of the ImageCLEF 2021: Multimedia Retrieval in Medical, Nature, Internet and Social Media Applications”. In: *Experimental IR Meets Multilinguality, Multimodality, and Interaction*. 2021, pp. 345–370. URL: https://link.springer.com/chapter/10.1007/978-3-030-85251-1_23.

[Irv+19] Jeremy A. Irvin et al. “CheXpert: A Large Chest Radiograph Dataset with Uncertainty Labels and Expert Comparison”. In: *AAAI Conference on Artificial Intelligence*. 2019. URL: <https://api.semanticscholar.org/CorpusID:58981871>.

[Jeo+23] Jaehwan Jeong et al. *Multimodal Image-Text Matching Improves Retrieval-based Chest X-Ray Report Generation*. 2023. arXiv: 2303.17579.

[Ji20] Qiang Ji. “5 - Computer vision applications”. In: *Probabilistic Graphical Models for Computer Vision*. Computer Vision and Pattern Recognition. 2020, pp. 191–297. DOI: <https://doi.org/10.1016/B978-0-12-803467-5.00010-1>. URL: <https://www.sciencedirect.com/science/article/pii/B9780128034675000101>.

[Jia+21] Chao Jia et al. “Scaling Up Visual and Vision-Language Representation Learning with Noisy Text Supervision”. In: *International Conference on Machine Learning*. 2021.

[Jia+23] Albert Q. Jiang et al. *Mistral 7B*. 2023. arXiv: 2310.06825.

[Jin+21] Di Jin et al. “What Disease does This Patient Have? A Large-Scale Open Domain Question Answering Dataset from Medical Exams”. In: *Applied Sciences* 11.14 (2021), p. 6421.

[Jin+19] Qiao Jin et al. “PubMedQA: A Dataset for Biomedical Research Question Answering”. In: *Conference on Empirical Methods in Natural Language Processing*. 2019. URL: <https://api.semanticscholar.org/CorpusID:202572622>.

[Joh+19a] Alistair E. W. Johnson et al. *MIMIC-CXR-JPG, a Large Publicly Available Database of Labeled Chest Radiographs*. 2019. arXiv: 1901.07042.

[Joh+19b] Alistair EW Johnson et al. “MIMIC-CXR, a De-Identified Publicly Available Database of Chest Radiographs with Free-Text Reports”. In: *Scientific Data* 6 (2019).

[Kay+22] Maxime Kayser et al. “Explaining Chest X-ray Pathologies in Natural Language”. In: *International Conference on Medical Image Computing and Computer-Assisted Intervention (MICCAI)*. Vol. 13435. 2022, pp. 701–713. URL: https://doi.org/10.1007/978-3-031-16443-9_67.

[KJZ18] Jin-Hwa Kim, Jaehyun Jun, and Byoung-Tak Zhang. “Bilinear Attention Networks”. In: *Advances in Neural Information Processing Systems 31*. 2018, pp. 1571–1581. URL: https://proceedings.neurips.cc/paper_files/paper/2018/file/96ea64f3a1aa2fd00c72faacf0cb8ac9-Paper.pdf.

[KB14] Diederik P. Kingma and Jimmy Ba. “Adam: A Method for Stochastic Optimization”. In: *International Conference on Learning Representations* abs/1412.6980 (2014).

[Kwo+23] Gukyeong Kwon et al. *Masked Vision and Language Modeling for Multi-modal Representation Learning*. 2023. arXiv: 2208.02131.

[Lan+19] Zhenzhong Lan et al. “ALBERT: A Lite BERT for Self-Supervised Learning of Language Representations”. In: *International Conference on Learning Representations*. 2019.

[Lau+18] Jason J Lau et al. “A Dataset of Clinically Generated Visual Questions and Answers about Radiology Images”. In: *Scientific data* 5.1 (2018), pp. 1–10. URL: <https://www.nature.com/articles/sdata2018251>.

[Lee+23] Hyungyung Lee et al. *UniXGen: A Unified Vision-Language Model for Multi-View Chest X-ray Generation and Report Generation*. 2023. arXiv: 2302.12172.

[LAC21] Brian Lester, Rami Al-Rfou, and Noah Constant. *The Power of Scale for Parameter-Efficient Prompt Tuning*. 2021. arXiv: 2104.08691.

[Lew+20] Patrick Lewis et al. “Retrieval-Augmented Generation for Knowledge-Intensive NLP Tasks”. In: *Neural Information Processing Systems*. 2020. URL: <https://dl.acm.org/doi/10.5555/3495724.3496517>.

[Li+23a] Chunyuan Li et al. *LLaVA-Med: Training a Large Language-and-Vision Assistant for Biomedicine in One Day*. 2023. arXiv: 2306.00890.

[Li+21] Junnan Li et al. “Align Before Fuse: Vision and Language Representation Learning with Momentum Distillation”. In: *Advances in Neural Information Processing Systems*. 2021. URL: <https://proceedings.neurips.cc/paper/2021/file/505259756244493872b7709a8a01b536-Paper.pdf>.

[Li+19] Liunian Harold Li et al. *VisualBERT: A Simple and Performant Baseline for Vision and Language*. 2019. arXiv: 1908.03557.

[Li+22] Mingjie Li et al. “Cross-modal Clinical Graph Transformer for Ophthalmic Report Generation”. In: *IEEE/CVF Conference on Computer Vision and Pattern Recognition (CVPR)*. 2022, pp. 20624–20633. DOI: 10.1109/CVPR52688.2022.02000.

[Li+23b] Pengfei Li et al. “Masked Vision and Language Pre-Training with Unimodal and Multimodal Contrastive Losses for Medical Visual Question Answering”. In: *Medical Image Computing and Computer Assisted Intervention (MICCAI)*. 2023, pp. 374–383. URL: https://link.springer.com/chapter/10.1007/978-3-031-43907-0_36.

[LL21] Xiang Lisa Li and Percy Liang. *Prefix-Tuning: Optimizing Continuous Prompts for Generation*. 2021. arXiv: 2101.00190.

[Li+23c] Yunxiang Li et al. “ChatDoctor: A Medical Chat Model Fine-Tuned on a Large Language Model Meta-AI (LLaMA) Using Medical Domain Knowledge”. In: *Cureus* 15.6 (2023). URL: <https://www.cureus.com/articles/152858-chatdoctor-a-medical-chat-model-fine-tuned-on-a-large-language-model-meta-ai-llama-using-medical-domain-knowledge#!/>.

[Lin04] Chin-Yew Lin. “ROUGE: A Package for Automatic Evaluation of Summaries”. In: *Text Summarization Branches Out*. 2004, pp. 74–81. URL: <https://aclanthology.org/W04-1013>.

[Lin+23a] Weixiong Lin et al. *PMC-CLIP: Contrastive Language-Image Pre-Training using Biomedical Documents*. 2023. arXiv: 2303.07240.

[Lin+23b] Zhihong Lin et al. “Medical Visual Question Answering: A Survey”. In: *Artificial Intelligence in Medicine* 143 (2023), p. 102611. DOI: 10.1016/j.artmed.2023.102611. URL: <http://dx.doi.org/10.1016/j.artmed.2023.102611>.

[Liu+23a] Bo Liu et al. “Medical Visual Question Answering via Conditional Reasoning and Contrastive Learning”. In: *IEEE Transactions on Medical Imaging* 42.5 (2023), pp. 1532–1545. DOI: 10.1109/TMI.2022.3232411.

[Liu+21a] Bo Liu et al. “Slake: A Semantically-Labeled Knowledge-Enhanced Dataset for Medical Visual Question Answering”. In: *IEEE 18th International Symposium on Biomedical Imaging (ISBI)* (2021), pp. 1650–1654. URL: <https://api.semanticscholar.org/CorpusID:231951663>.

[LTS23] Chang Liu, Yuanhe Tian, and Yan Song. *A Systematic Review of Deep Learning-based Research on Radiology Report Generation*. 2023. arXiv: 2311.14199.

[Liu+22] Fangyu Liu et al. *DePlot: One-Shot Visual Language Reasoning by Plot-to-Table Translation*. 2022. arXiv: 2212.10505.

[Liu+24] Hanchao Liu et al. *A Survey on Hallucination in Large Vision-Language Models*. 2024. arXiv: 2402.00253.

[Liu+23b] Haotian Liu et al. *Visual Instruction Tuning*. 2023. arXiv: 2304.08485.

[Liu+21b] Ze Liu et al. “Swin Transformer: Hierarchical Vision Transformer using Shifted Windows”. In: *International Conference on Computer Vision (ICCV)*. 2021, pp. 9992–10002. DOI: 10.1109/ICCV48922.2021.00986. URL: <https://doi.ieee.org/10.1109/ICCV48922.2021.00986>.

[Lo+20] Kyle Lo et al. “S2ORC: The Semantic Scholar Open Research Corpus”. In: *Annual Meeting of the Association for Computational Linguistics*. 2020, pp. 4969–4983. DOI: 10.18653/v1/2020.acl-main.447. URL: <https://aclanthology.org/2020.acl-main.447>.

[Lu+19] Jiasen Lu et al. “ViLBERT: Pretraining Task-Agnostic Visiolinguistic Representations for Vision-and-Language Tasks”. In: *Advances in Neural Information Processing Systems*. 2019. URL: <https://api.semanticscholar.org/CorpusID:199453025>.

[MHC20] Thusitha Mabotuwana, Christopher S Hall, and Nathan Cross. “Framework for Extracting Critical Findings in Radiology Reports”. In: *Journal of Digital Imaging* 33.4 (2020). URL: <https://link.springer.com/article/10.1007/s10278-020-00349-7>.

[Mah+22] Supriya Mahadevkar et al. “A Review on Machine Learning Styles in Computer Vision - Techniques and Future Directions”. In: *IEEE Access* 10 (2022), pp. 107293–107329. DOI: [10.1109/ACCESS.2022.3209825](https://doi.org/10.1109/ACCESS.2022.3209825).

[Man+23] Omid Nejati Manzari et al. “MedViT: A Robust Vision Transformer for Generalized Medical Image Classification”. In: *Computers in Biology and Medicine* 157 (2023), p. 106791. DOI: <https://doi.org/10.1016/j.combiomed.2023.106791>. URL: <https://www.sciencedirect.com/science/article/pii/S0010482523002561>.

[Mas+11] Jonathan Masci et al. “Stacked Convolutional Auto-Encoders for Hierarchical Feature Extraction”. In: *International Conference on Artificial Neural Networks*. 2011. URL: <https://api.semanticscholar.org/CorpusID:12640199>.

[Mik+13a] Tomas Mikolov et al. “Distributed Representations of Words and Phrases and Their Compositionality”. In: *Advances in Neural Information Processing Systems*. Vol. 26. 2013.

[Mik+13b] Tomas Mikolov et al. *Distributed Representations of Words and Phrases and their Compositionality*. 2013. arXiv: [1310.4546](https://arxiv.org/abs/1310.4546).

[Mik+13c] Tomas Mikolov et al. *Efficient Estimation of Word Representations in Vector Space*. 2013. arXiv: [1301.3781](https://arxiv.org/abs/1301.3781).

[Mis+21] Pankaj Mishra et al. “VT-ADL: A Vision Transformer Network for Image Anomaly Detection and Localization”. In: *IEEE International Symposium on Industrial Electronics (ISIE)*. 2021, pp. 01–06. URL: <https://api.semanticscholar.org/CorpusID:233307063>.

[Miu+21] Yasuhide Miura et al. “Improving Factual Completeness and Consistency of Image-to-Text Radiology Report Generation”. In: *North American Chapter of the Association for Computational Linguistics*. 2021, pp. 5288–5304. DOI: [10.18653/v1/2021.naacl-main.416](https://doi.org/10.18653/v1/2021.naacl-main.416). URL: <https://aclanthology.org/2021.naacl-main.416>.

[Moo+22] Jong Hak Moon et al. “Multi-Modal Understanding and Generation for Medical Images and Text via Vision-Language Pre-Training”. In: *IEEE Journal of Biomedical and Health Informatics* 26.12 (2022), pp. 6070–6080. DOI: [10.1109/JBHI.2022.3207502](https://doi.org/10.1109/JBHI.2022.3207502).

[Moo+23] Michael Moor et al. *Med-Flamingo: A Multimodal Medical Few-Shot Learner*. 2023. arXiv: [2307.15189](https://arxiv.org/abs/2307.15189).

[OLV19] Aaron van den Oord, Yazhe Li, and Oriol Vinyals. *Representation Learning with Contrastive Predictive Coding*. 2019. arXiv: [1807.03748](https://arxiv.org/abs/1807.03748).

[Pap+02] Kishore Papineni et al. “Bleu: a Method for Automatic Evaluation of Machine Translation”. In: *Annual Meeting of the Association for Computational Linguistics*. 2002. URL: <https://api.semanticscholar.org/CorpusID:11080756>.

[Par+22] Darsh Parekh et al. “A Review on Autonomous Vehicles: Progress, Methods and Challenges”. In: *Electronics* 11.14 (2022). DOI: [10.3390/electronics11142162](https://doi.org/10.3390/electronics11142162). URL: <https://www.mdpi.com/2079-9292/11/14/2162>.

[Pel+18] Obioma Pelka et al. “Radiology Objects in COntext (ROCO): A Multimodal Image Dataset”. In: *Intravascular Imaging and Computer Assisted Stenting and Large-Scale Annotation of Biomedical Data and Expert Label Synthesis*. Springer International Publishing, 2018, pp. 180–189. URL: https://link.springer.com/chapter/10.1007/978-3-030-01364-6_20.

[Pel+23] Chantal Pellegrini et al. *RaDialog: A Large Vision-Language Model for Radiology Report Generation and Conversational Assistance*. 2023. arXiv: 2311.18681.

[Pen+17] Yifan Peng et al. “NegBio: A High-Performance Tool for Negation and Uncertainty Detection in Radiology Reports”. In: *AMIA Summits on Translational Science Proceedings* 2018 (2017), pp. 188–196. URL: <https://api.semanticscholar.org/CorpusID:19572090>.

[PSM14] Jeffrey Pennington, Richard Socher, and Christopher Manning. “Glove: Global Vectors for Word Representation”. In: *Empirical Methods in Natural Language Processing*. Vol. 14. 2014, pp. 1532–1543. DOI: 10.3115/v1/D14-1162.

[Rad+21] Alec Radford et al. *Learning Transferable Visual Models from Natural Language Supervision*. 2021. arXiv: 2103.00020.

[RB21] Abigail Rai and Samarjeet Borah. “Study of Various Methods for Tokenization”. In: *Applications of Internet of Things*. 2021, pp. 193–200. DOI: https://doi.org/10.1007/978-981-15-6198-6_18.

[RCR22] Vignav Ramesh, Nathan Chi, and Pranav Rajpurkar. “Improving Radiology Report Generation Systems by Removing Hallucinated References to Non-existent Priors”. In: *Machine Learning Research*. Vol. 193. 2022, pp. 456–473. URL: <https://proceedings.mlr.press/v193/ramesh22a/ramesh22a.pdf>.

[RBK21] René Ranftl, Alexey Bochkovskiy, and Vladlen Koltun. “Vision Transformers for Dense Prediction”. In: *IEEE/CVF International Conference on Computer Vision (ICCV)*. 2021, pp. 12159–12168. URL: <https://api.semanticscholar.org/CorpusID:232352612>.

[Ran+23a] Veenu Rani et al. “Self-supervised Learning: A Succinct Review”. In: *Archives of Computational Methods in Engineering* 30 (2023). DOI: 10.1007/s11831-023-09884-2.

[Ran+23b] Mercy Ranjit et al. *Retrieval Augmented Chest X-Ray Report Generation using OpenAI GPT models*. 2023. arXiv: 2305.03660.

[Red+16] Joseph Redmon et al. “You Only Look Once: Unified, Real-Time Object Detection”. In: *2016 IEEE Conference on Computer Vision and Pattern Recognition (CVPR)*. 2016, pp. 779–788. DOI: 10.1109/CVPR.2016.91. URL: <https://doi.ieee.org/10.1109/CVPR.2016.91>.

[Ren+15] Shaoqing Ren et al. “Faster R-CNN: Towards Real-Time Object Detection with Region Proposal Networks”. In: *IEEE Transactions on Pattern Analysis and Machine Intelligence* 39 (2015), pp. 1137–1149. URL: <https://api.semanticscholar.org/CorpusID:10328909>.

[Rez+19] Seyed Hamid Rezatofighi et al. “Generalized Intersection Over Union: A Metric and a Loss for Bounding Box Regression”. In: *IEEE/CVF Conference on Computer Vision and Pattern Recognition (CVPR)* (2019), pp. 658–666.

[Rob51] Herbert E. Robbins. “A Stochastic Approximation Method”. In: *Annals of Mathematical Statistics* 22 (1951), pp. 400–407.

[RS18] Alexey Romanov and Chaitanya Shivade. “Lessons from Natural Language Inference in the Clinical Domain”. In: *Conference on Empirical Methods in Natural Language Processing*. 2018, pp. 1586–1596. DOI: 10.18653/v1/D18-1187. URL: <https://aclanthology.org/D18-1187>.

[RFB15] Olaf Ronneberger, Philipp Fischer, and Thomas Brox. “U-Net: Convolutional Networks for Biomedical Image Segmentation”. In: *Medical Image Computing and Computer-Assisted Intervention – MICCAI*. 2015, pp. 234–241. ISBN: 978-3-319-24574-4.

[Rüc+22] Johannes Rückert et al. “Overview of ImageCLEFmedical 2022 – Caption Prediction and Concept Detection”. In: *Conference and Labs of the Evaluation Forum (CLEF)*. 2022.

[Sch19] Robin M. Schmidt. *Recurrent Neural Networks (RNNs): A gentle Introduction and Overview*. 2019. arXiv: 1912.05911.

[See+22] Lalithkumar Seenivasan et al. “Surgical-VQA: Visual Question Answering in Surgical Scenes Using Transformer”. In: *Medical Image Computing and Computer Assisted Intervention – MICCAI*. 2022, pp. 33–43.

[SB23] Saurav Sengupta and Donald E. Brown. *Automatic Report Generation for Histopathology images using pre-trained Vision Transformers and BERT*. 2023. arXiv: 2312.01435.

[SHB16] Rico Sennrich, Barry Haddow, and Alexandra Birch. “Neural Machine Translation of Rare Words with Subword Units”. In: *54th Annual Meeting of the Association for Computational Linguistics (Volume 1: Long Papers)*. 2016, pp. 1715–1725. DOI: 10.18653/v1/P16-1162. URL: <https://aclanthology.org/P16-1162>.

[SDK23] Dhruv Sharma, Chhavi Dhiman, and Dinesh Kumar. “Evolution of Visual Data Captioning Methods, Datasets, and Evaluation Metrics: a Comprehensive Survey”. In: *Expert Systems with Applications* 221 (2023), p. 119773. ISSN: 0957-4174. DOI: <https://doi.org/10.1016/j.eswa.2023.119773>. URL: <https://www.sciencedirect.com/science/article/pii/S0957417423002749>.

[Sho+19] Mohammad Shoeybi et al. *Megatron-LM: Training Multi-Billion Parameter Language Models Using Model Parallelism*. 2019. arXiv: 1909.08053.

[Shr+23] Prashant Shrestha et al. *Medical Vision Language Pretraining: A survey*. 2023. arXiv: 2312.06224.

[Shu+23] Chang Shu et al. *Visual Med-Alpaca: A Parameter-Efficient Biomedical LLM with Visual Capabilities*. [Online; accessed 20-Feb-2024]. 2023. URL: <https://cambridgel1.github.io/visual-med-alpaca/>.

[Sin+23] Karan Singhal et al. “Large Language Models Encode Clinical Knowledge”. In: *Nature* 620 (2023), pp. 172–180.

[Smi+20] Akshay Smit et al. *CheXbert: Combining Automatic Labelers and Expert Annotations for Accurate Radiology Report Labeling Using BERT*. 2020. arXiv: 2004.09167.

[Sov+21] Petru Soviany et al. “Curriculum Learning: A Survey”. In: *International Journal of Computer Vision* 130 (2021), pp. 1526–1565. URL: <https://api.semanticscholar.org/CorpusID:231709290>.

[Sub+20] Sanjay Subramanian et al. “MedICaT: A Dataset of Medical Images, Captions, and Textual References”. In: *Findings of EMNLP*. 2020.

[Sun+23] Zhiqing Sun et al. *Aligning Large Multimodal Models with Factually Augmented RLHF*. 2023. arXiv: 2309.14525.

[TL20] Mingxing Tan and Quoc V. Le. *EfficientNet: Rethinking Model Scaling for Convolutional Neural Networks*. 2020. arXiv: 1905.11946.

[TBF22] Ajay K. Tanwani, Joelle Barral, and Daniel Freedman. “RepsNet: Combining Vision with Language for Automated Medical Reports”. In: *Medical Image Computing and Computer Assisted Intervention (MICCAI)*. 2022, pp. 714–724. DOI: https://doi.org/10.1007/978-3-031-16443-9_68.

[Tay53] Wilson L. Taylor. ““Cloze Procedure”: A New Tool for Measuring Readability”. In: *Journalism & Mass Communication Quarterly* 30 (1953), pp. 415–433.

[Tha+23] Omkar Thawkar et al. *XrayGPT: Chest Radiographs Summarization using Medical Vision-Language Models*. 2023. arXiv: 2306.07971.

[TLZ23] Pang Ting, Peigao Li, and Lijie Zhao. “A Survey on Automatic Generation of Medical Imaging Reports based on Deep Learning”. In: *BioMedical Engineering OnLine* 22 (May 2023). DOI: 10.1186/s12938-023-01113-y.

[Tou+23a] Hugo Touvron et al. *Llama 2: Open Foundation and Fine-Tuned Chat Models*. 2023. arXiv: 2307.09288.

[Tou+23b] Hugo Touvron et al. *LLaMA: Open and Efficient Foundation Language Models*. 2023. arXiv: 2302.13971.

[Tou+21] Hugo Touvron et al. “Training Data-Efficient Image Transformers & Distillation through Attention”. In: *The International Conference on Machine Learning*. Vol. 139. 2021, pp. 10347–10357. URL: <https://proceedings.mlr.press/v139/touvron21a.html>.

[Tri+23] Aakash Tripathi et al. *Building Flexible, Scalable, and Machine Learning-ready Multimodal Oncology Datasets*. 2023. arXiv: 2310.01438.

[Tya+21] Khushal Tyagi et al. “Detecting Pneumonia using Vision Transformer and Comparing with Other Techniques”. In: *International Conference on Electronics, Communication and Aerospace Technology (ICECA)*. 2021, pp. 12–16. DOI: 10.1109/ICECA52323.2021.9676146.

[Vas+17] Ashish Vaswani et al. “Attention Is All You Need”. In: *Advances in Neural Information Processing Systems*. Vol. 30. 2017.

[VC13] Karin Verspoor and Kevin Bretonnel Cohen. “Natural Language Processing”. In: *Encyclopedia of Systems Biology*. Springer New York, 2013, pp. 1495–1498. DOI: 10.1007/978-1-4419-9863-7_158. URL: https://doi.org/10.1007/978-1-4419-9863-7_158.

[WCG20] Changhan Wang, Kyunghyun Cho, and Jiatao Gu. “Neural Machine Translation with Byte-Level Subwords”. In: *AAAI Conference on Artificial Intelligence*. 2020, pp. 9154–9160.

[Wan+22a] Jianfeng Wang et al. *GIT: A Generative Image-to-text Transformer for Vision and Language*. 2022. arXiv: 2205.14100.

[Wan+23a] Liyuan Wang et al. *A Comprehensive Survey of Continual Learning: Theory, Method and Application*. 2023. arXiv: 2302.00487.

[Wan+23b] Yizhong Wang et al. *Self-Instruct: Aligning Language Models with Self-Generated Instructions*. 2023. arXiv: 2212.10560.

[Wan+22b] Zifeng Wang et al. *MedCLIP: Contrastive Learning from Unpaired Medical Images and Text*. 2022. arXiv: 2210.10163.

[Wan+22c] Zirui Wang et al. “SimVLM: Simple Visual Language Model Pretraining with Weak Supervision”. In: *International Conference on Learning Representations (ICLR)*. 2022.

[Waq+23] Asim Waqas et al. *Multimodal Data Integration for Oncology in the Era of Deep Neural Networks: A Review*. 2023. arXiv: 2303.06471.

[Wu+19] Huikai Wu et al. *FastFCN: Rethinking Dilated Convolution in the Backbone for Semantic Segmentation*. 2019. arXiv: 1903.11816.

[Wu+16] Yonghui Wu et al. *Google’s Neural Machine Translation System: Bridging the Gap between Human and Machine Translation*. 2016. arXiv: 1609.08144.

[Xie+16] Saining Xie et al. “Aggregated Residual Transformations for Deep Neural Networks”. In: *IEEE Conference on Computer Vision and Pattern Recognition (CVPR)* (2016), pp. 5987–5995. URL: <https://api.semanticscholar.org/CorpusID:8485068>.

[Xie+22] Zhenda Xie et al. “SimMIM: A Simple Framework for Masked Image Modeling”. In: *IEEE/CVF Conference on Computer Vision and Pattern Recognition (CVPR)* (2022), pp. 9643–9653. URL: <https://api.semanticscholar.org/CorpusID:244346275>.

[Xin+22] Chao Xin et al. “An Improved Transformer Network for Skin Cancer Classification”. In: *Computers in Biology and Medicine* 149 (2022), p. 105939. DOI: <https://doi.org/10.1016/j.combiomed.2022.105939>. URL: <https://www.sciencedirect.com/science/article/pii/S001048252200674>.

[Xu+21] Mengya Xu et al. “Learning Domain Adaptation with Model Calibration for Surgical Report Generation in Robotic Surgery”. In: *2021 IEEE International Conference on Robotics and Automation (ICRA)* (2021), pp. 12350–12356.

[Yam+18] Rikiya Yamashita et al. “Convolutional Neural Networks: an Overview and Application in Radiology”. In: *Insights into Imaging* 9 (June 2018). DOI: 10.1007/s13244-018-0639-9.

[Yan+22] Xi Yang et al. “A Large Language Model for Electronic Health Records”. In: *NPJ Digital Medicine* 5 (2022). URL: <https://api.semanticscholar.org/CorpusID:255175535>.

[Yan+16] Zichao Yang et al. “Hierarchical Attention Networks for Document Classification”. In: *Conference of the North American Chapter of the Association for Computational Linguistics: Human Language Technologies*. 2016, pp. 1480–1489. DOI: 10.18653/v1/N16-1174. URL: <https://aclanthology.org/N16-1174>.

[Yu+23] Feiyang Yu et al. “Evaluating Progress in Automatic Chest X-ray Radiology Report Generation”. In: *Patterns* 4 (Aug. 2023), p. 100802. DOI: 10.1016/j.patter.2023.100802.

[Yua+23] Zheng Yuan et al. *RAMM: Retrieval-augmented Biomedical Visual Question Answering with Multi-modal Pre-training*. 2023. arXiv: 2303.00534.

[Zel+19] Rowan Zellers et al. “From Recognition to Cognition: Visual Commonsense Reasoning”. In: *IEEE/CVF Conference on Computer Vision and Pattern Recognition (CVPR)*. 2019, pp. 6713–6724. DOI: 10.1109/CVPR.2019.00688.

[Zen+20] Guangtao Zeng et al. “MedDialog: Large-scale Medical Dialogue Datasets”. In: *Conference on Empirical Methods in Natural Language Processing (EMNLP)*. 2020, pp. 9241–9250. DOI: 10.18653/v1/2020.emnlp-main.743. URL: <https://aclanthology.org/2020.emnlp-main.743>.

[Zha+23a] Yuexiang Zhai et al. *Investigating the Catastrophic Forgetting in Multimodal Large Language Models*. 2023. arXiv: 2309.10313.

[Zha+20a] Li-Ming Zhan et al. “Medical Visual Question Answering via Conditional Reasoning”. In: *The 28th ACM International Conference on Multimedia*. 2020. URL: <https://ieeexplore.ieee.org/document/9999450?denied=>.

[ZNC18] Hanwang Zhang, Yulei Niu, and Shih-Fu Chang. “Grounding Referring Expressions in Images by Variational Context”. In: *IEEE/CVF Conference on Computer Vision and Pattern Recognition*. 2018, pp. 4158–4166. DOI: 10.1109/CVPR.2018.00437.

[Zha+23b] Sheng Zhang et al. *Large-Scale Domain-Specific Pretraining for Biomedical Vision-Language Processing*. 2023. arXiv: 2303.00915.

[Zha+20b] Tianyi Zhang et al. “BERTScore: Evaluating Text Generation with BERT”. In: *International Conference on Learning Representations*. 2020. URL: <https://openreview.net/forum?id=SkeHuCVFDr>.

[Zha+23c] Wentao Zhang et al. *Adapter Learning in Pretrained Feature Extractor for Continual Learning of Diseases*. 2023. arXiv: 2304.09042.

[Zha+19] Yijia Zhang et al. “BioWordVec, Improving Biomedical Word Embeddings with Subword Information and MeSH”. In: *Scientific Data* 6 (2019).

[Zha+23d] Ruochen Zhao et al. *Retrieving Multimodal Information for Augmented Generation: A Survey*. 2023. arXiv: 2303.10868.

[Zhe+19] Liangli Zhen et al. “Deep Supervised Cross-Modal Retrieval”. In: *IEEE/CVF Conference on Computer Vision and Pattern Recognition (CVPR)*. 2019, pp. 10386–10395. DOI: 10.1109/CVPR.2019.01064.

[Zho+23a] Hongjian Zhou et al. *A Survey of Large Language Models in Medicine: Progress, Application, and Challenge*. 2023. arXiv: 2311.05112.

[Zho+23b] Da-Wei Zhou et al. *Learning without Forgetting for Vision-Language Models*. 2023. arXiv: 2305.19270.